

### 3 Marine Geological Investigations

(R. Stein, S. Drachev, K. Fahl, J. Hefter, H. Kassens, N. Koukina, J. Matthiessen, C. Müller, E. Musatov, J. Mutterlose, N. Nörsgaard-Petersen, K. Polozek, V. Shevchenko and R. Usbeck)

The overall goals of the marine-geological research program are

- (1) high-resolution studies of changes in paleoclimate, paleoceanic circulation, paleoproductivity, and sea-ice distribution in the central Arctic Ocean and the adjacent continental margin during Late Quaternary times, and
- (2) the long-term history of the Mesozoic and Cenozoic Arctic Ocean and its environmental evolution from a warm polar ocean to an ice-covered polar ocean.

In areas such as the Alpha-Mendeleev-Ridge, pre-Quaternary sediments are cropping out (e. g., Jackson et al., 1985; Clark et al., 1986), which could even be cored with coring gears aboard RV POLARSTERN and which would allow to study the Tertiary/Cretaceous history of the (preglacial) Arctic Ocean. Especially the available data for the reconstruction of the long-term paleoclimatic history of the Arctic Ocean are very rare and only based on very short sediment cores taken from drifting ice islands.

Thus, the main working area on the Alpha-Ridge has been chosen between 84 and 86°N and 95 and 140°W. In this area, four short cores from ice islands containing lower Tertiary/Upper Cretaceous sediments were obtained from the ice island T3 and during the CESAR-Expedition (Clark et al., 1980; Jackson et al., 1985) (Fig. 11):

Core FL533:	85° 05.9'N, 98° 17.8'W	Lower Mastrichtian
Core FL437:	85° 59.5'N, 129° 58.5'W	Late Mastrichtian
Core FL422:	84° 53.3'N, 124° 32.5'W	Middle Eocene
Core CESAR-6:	85° 49.6'N, 109° 04.9'W	Late Mastrichtian

Due to too strong ice conditions, unfortunately, this area of the Alpha Ridge could not be reached by RV POLARSTERN, and the main study area on the Alpha Ridge has had to be shifted to the western part of the ridge (Fig. 11).

During ARK-XIV/1a, surface and sub-surface sediment samples were taken by the giant box corer, the multicorer, the kastenlot corer, and the gravity corer. In general, coring positions were carefully selected using PARASOUND to avoid areas of sediment redeposition and erosion. In addition, snow fields, dirty-sea-ice areas, melt ponds as well as the upper 75 m of the water column were sampled. During transit times, aerosols were routinely collected using a pump installed on the uppermost deck of the vessel.

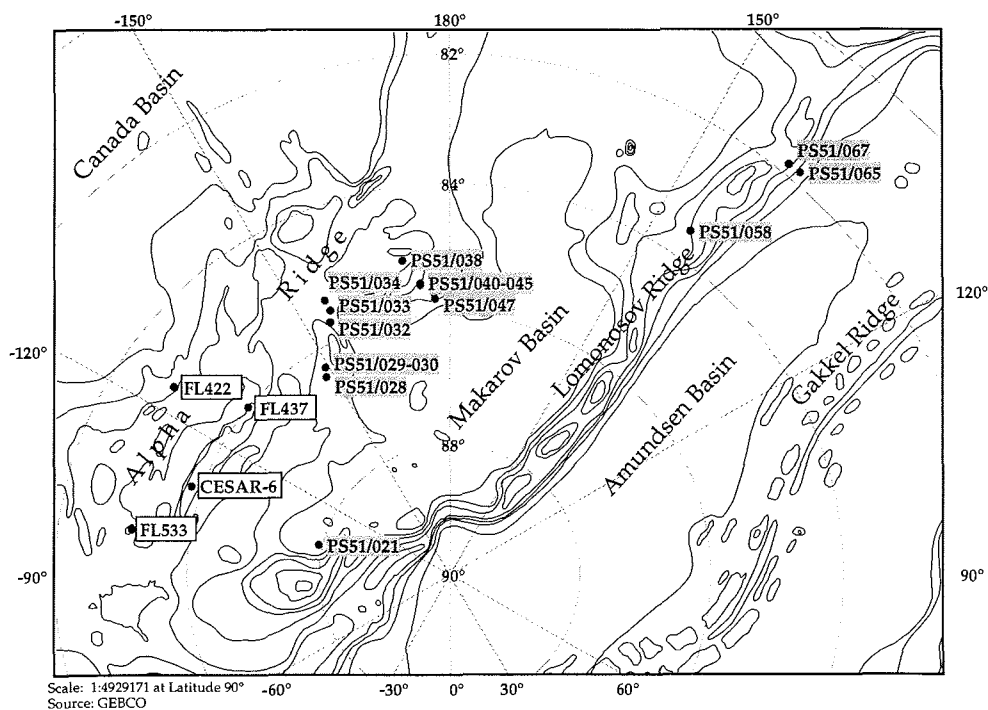


Fig. 11: Location of geological sampling stations performed during the ARK-XIV/1a Expedition. In addition, the location of the four cores taken from ice island T3 and during the CEASR-Expedition are shown. At these four locations lower Tertiary/Upper Cretaceous sediments were recovered.

The scientific investigations to be performed in the different laboratories will concentrate on:

- high-resolution stratigraphic analyses of the sediment sequences (isotopic stratigraphy, AMS 14-C-datings, amino-acids, magnetic susceptibility);
- studies of terrigenous sediment supply (grain size; clay, light, and heavy minerals; organic compounds; geochemical tracers);
- studies of the fluxes of terrigenous and marine organic carbon (total organic carbon, C/N ratios, hydrogen and oxygen indices, stable carbon and nitrogen isotopes, maceral composition, biomarker);

- reconstruction of paleoproductivity by tracer analyses (biomarkers, biogenic opal, stable isotopes, etc.);
- studies of reactions of marine biota to long- and short-term environmental changes;
- studies of physical properties (magnetic susceptibility, wet bulk density, porosity, shear strength);
- study of composition and grain size of aerosol particles;
- study of specific sedimentary environments with detailed PARASOUND surveys.

### 3.1 High resolution acoustic profiling by the PARASOUND echosounder system (S. Drachev, R. Usbeck)

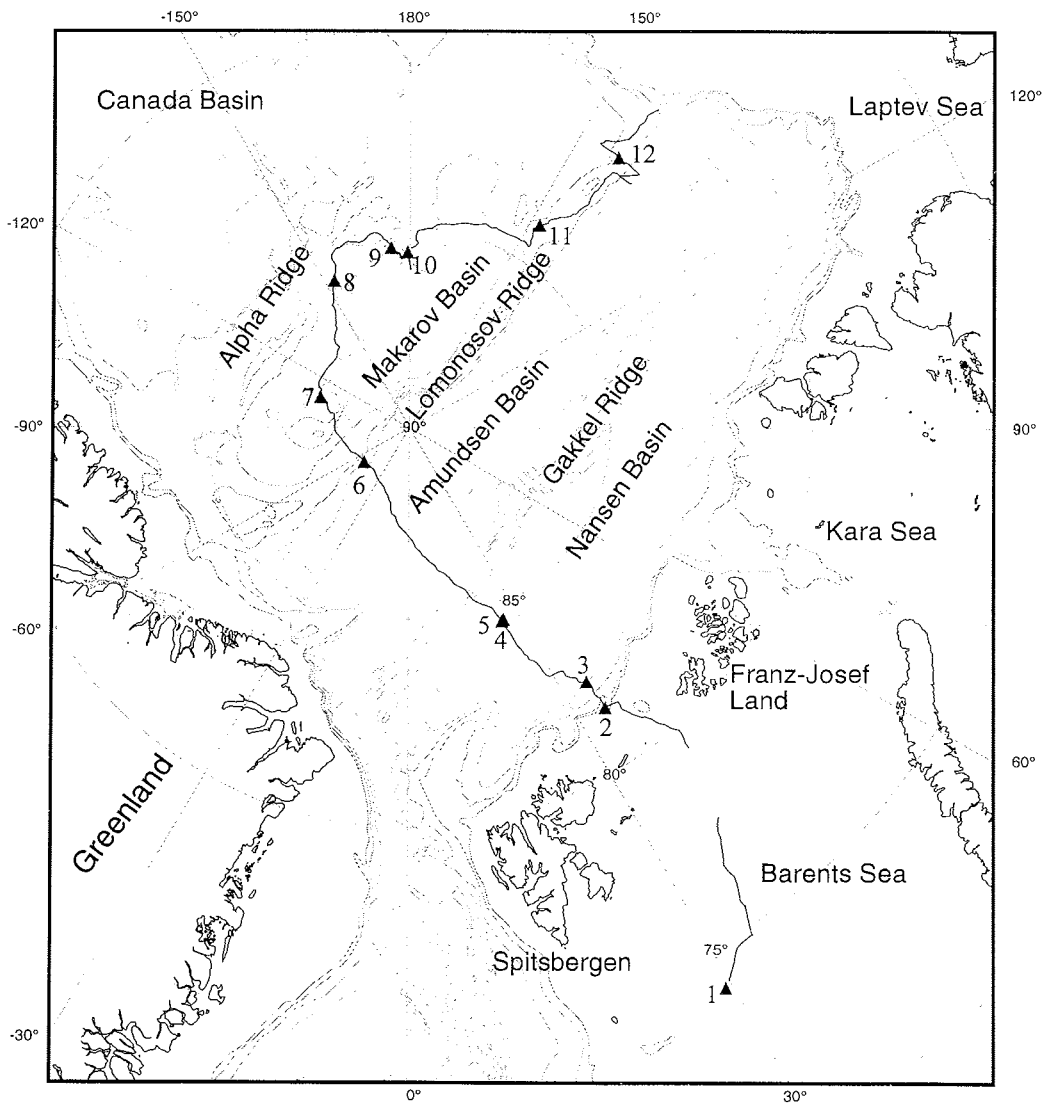
The PARASOUND is an echosounding-type device designed to acquire a high resolution acoustic record of sub-bottom sediments. This record can be interpreted in terms of structural and facial characteristics of the sediments. According to the research program of the ARK XIV/1a cruise, the PARASOUND profiling aimed at:

- acquiring information from sub-bottom reflections for the selection of relevant sites for sampling of the sediments by gravity and kastenlot corers;
- providing a two- or even three-dimensional stratigraphic framework for lateral correlation of the sediment cores based on the sub-bottom reflection pattern;
- detecting changes in sediment facies along the transect from Spitsbergen to the Alpha Ridge and back to the continental slope of the Laptev Sea by means of interpretation of the high resolution acoustic record.

We started to run the PARASOUND on July 2nd at 74°01.5' N, 29°37.8' E south of Spitsbergen and kept it in 24-hour operation along the ship track until the end of the cruise on July 24th at 79°56.5' N, 142°07.1' E north of the New Siberian Islands (Fig. 12). This continuous profiling was interrupted only once in the Barents Shelf area between 75°50' N, 35°00' E and 81°28' N, 35°00' E where we entered the Russian economic zone, were not permitted to carry out any measurements. The following is a brief description of the obtained data and a preliminary discussion of the results.

#### 3.1.1. Data acquisition system and data description

The PARASOUND system (Krupp Atlas Electronics, Bremen, Germany) generates two primary frequencies between 18 and 23.5 kHz transmitting in a narrow beam of 4°. As a result of the interaction of the primary frequencies within the water column, a secondary frequency is created based on the parametric effect. The parametric frequency is the difference frequency of the two primary waves transmitted. During ARK-XIV/1a cruise the parametric frequency was set to 4 kHz. This allowed sub-bottom penetration up to 100 m with a vertical resolution of ca. 30 cm. The



▲ Start points of DESO rolls No.

Fig. 12: Cruise track and location of the DESO paper rolls/PARASOUND profiles.

parametric pulse length was set to 2 under normal operating conditions. Under extreme conditions, such as above steep slopes and while operating in heavy sea ice, the pulse length was increased up to 8. Recorded seismograms were independently digitised by two different systems: (i) by the PARASOUND system for simultaneous printing on a chart recorder (Atlas DESO 25) and (ii) by the PARADIGMA system (Spiess, 1992) for tape storage (DAT-tapes) and post-processing. The settings of the PARADIGMA system were as follows: sampling rate 25  $\mu$ s, trace length 133 or 266 ms, block size 10640 byte, format "SEG-Y packed" (Spiess, 1992).

As noted earlier (Thiede, 1988), the ship operations in sea ice covered areas produce a noise in the 3.5 - 4.5 kHz band which significantly disturbs the echosounding data. The level of this ice-breaking related noise depends on the thickness of the sea ice. Moreover, data disturbances are also related to frequent ice ramming of the vessel. Since most of the cruise took place in extremely heavy ice conditions, the PARASOUND data are strongly influenced by this kind of noise.

The complexity of the sea-bottom morphology is another strict factor which greatly limits the proper work of the PARASOUND. The operation above underwater ridges usually resulted in long-term losses of the signal and, consequently, the data.

Thus, both morphology of the sea-bottom and ice conditions caused very diverse quality of the PARASOUND data. Table 5 contains some general characteristics of the data revealed from the DESO analogue records. The location of the rolls/profiles is given in Figure 12. To estimate the data quality, we undertook a visual control of the quality of the analogue record. We applied a four-level scale of quality as follows:

- Very good quality, i. e. whole roll contains a continuous readable record slightly disturbed by ice-breaking related noise.
- Good quality, i. e. most of the roll contains a readable record disturbed by short intervals of data loss and ice-breaking related noise.
- Poor quality, i. e. most of the roll contains unreadable records, and the rare readable intervals are divided by long intervals of data missing.
- Very poor quality, i. e. almost the whole roll contains no readable records.

As follows from Table 5, the quality of the data strictly depends on the morphology of the crossed structural elements. When morphology is simple and flat, the quality of data is very good and good. These are the Barents continental shelf, Nansen, Amundsen and Makarov deep oceanic basins, and some crestal parts of the Lomonosov Ridge. In contrast, the positive structures, whose morphology is complex and variable due to presence of numerous steep slopes, reveal poor and very poor data quality. These are the Gakkel Ridge, Alpha Ridge and most of the Lomonosov Ridge.

Tab. 5: PARASOUND data characteristics

DESO paper rolls 1	Start of record: date/time, GMT latitude, longitude	End of record: date/time, GMT latitude, longitude	DAT-Tapes 1	Morphological province	Range of penetration, m	Quality, visual estimation
1	02.07.98/23:06 74°01.5' N 29°37.8' E	04.07.98/03:00 75°50.0' N 35°13.5' E	2-10	Barents Shelf	0-22	very good
2	05.07.98/17:20 81°28.5' N 34°53.4' E	06.07.98/08:21 82°11.8' N 35°10.8' E	10-12	Barents continental slope and rise	5-20	poor
3	06.07.98/09:03 82°16.4' N 34°45.2' E	07.07.98/14:45 84°04.2' N 26°12.3' E	12-16	Barents continental rise	4-25	poor
				Nansen oceanic basin	10-50	good
4	07.07.98/14:45 84°04.2' N 26°12.3' E	07.07.98/19:58 84°39.6' N 25°30.1' E	16-18	Nansen oceanic basin	24-38	good
5	07.07.98/20:00 84°39.8' N 25°28.1' E	09.07.98/21:45 88°37.0' N 51°51.8' W	18-25	Nansen oceanic basin	25-40	good/poor
				Gakkel mid-oceanic ridge	5-30	very poor
				Amundsen oceanic basin	10-30	good/poor
6	09.07.98/21:50 88°36.9' N 52°29.2' W	11.07.98/15:15 87°42.0' N 109°08.6' W	25-29	Western Lomonosov Ridge	5-25	very poor
				Western Makarov Basin	15-50	poor and very poor
7	11.07.98/16:00 87°41.9' N 109°12.6' W	14.07.98/19:55 85°53.8' N 153°08.9' W	29-36	Northern slope of central Alpha Ridge	10-25	very poor
8	14.07.98/19:55 85°53.8' N 153°08.9' W	17.07.98/04:22 85°29.5' N 174°03.6' W	36-41	Eastern Alpha Ridge	2-50	very poor
9	17.07.98/04:22 85°29.5' N 174°03.6' W	19.07.98/02:50 85°37.3' N 178°58.3' W	41-43	Eastern Alpha Ridge	-	very poor, almost no record
10	19.07.98/04:15 85°37.2' N 179°11.7' W	21.07.98/02:35 84°01.8' N 147°48.0' E	43-49	Eastern Alpha Ridge	5-15	very poor
				Eastern Makarov Basin	30-50	good
				Eastern Lomonosov Ridge	10-40	very poor
11	21.07.98/02:45 84°00.7' N 147°41.9' E	23.07.98/07:37 81°30.2' N 142°22.0' E	49-55	Eastern Lomonosov Ridge	10-110	good/poor
12	23.07.98/07:45 81°30.2' N 142°28.6' E	24.07.98/09:35 79°56.6' N 142°07.6' E	55-57	Eastern Lomonosov Ridge	40-65	good

### 3.1.2 Regional description

This section contains some preliminary characteristics of the different structural elements in terms of their morphology and sedimentary pattern as consistent with the PARASOUND analogue record.

#### Barents continental margin

The Barents continental margin extends along the cruise track from the 74°01.5' N, 29°37.8' E to about 82°55' N, 28°51' E and contains the shelf, continental slope and continental rise areas (Fig. 12, Table 5).

A very good quality of the acoustic record was revealed on the Barents Shelf with the sound penetration down to 20 - 25 m below the sea bottom. There are two distinct acoustic units (App. 1). The upper acoustically transparent unit AU-1 mostly occurs within sea-bottom depressions. It rests on a sharp erosional surface which forms the top of another unit (AU-2). The penetration below this interface is in the range of a few meters and, thus, AU-2 can be interpreted as an acoustic basement. However, in some cases steep short reflectors were observed in top of AU-2 (App. 1 and App. 2). According to the well-known geology of this shelf, we suggest, that these acoustic units represent Quaternary glacial-marine sediments (AU-1) and deformed Mesozoic rocks (AU-2). The latter are often exposed on elevated parts of the sea-floor (App. 2) whose eroded or ice-ploughed surface becomes topographically complex due to numerous small positive and negative features with amplitude variations from 1 to 20 meters.

The shelf break is located at about 81°40.5' N, 35°07.3' E where the water depth reaches 350 - 360 m (App. 3). The upper continental slope is rather steep causing a poor penetration of the signal. However, the slope becomes gentle downward and the penetration increases to 30 m. The penetrated sediments are characterised by moderate to low reflectivity and are believed to consist of debris flow facies. Such sediments predominate in the continental rise area. App. 4 shows a sequence of fan levees composed of four individual sedimentary units with total thickness about 30 m. The upper 2 to 5 m of each unit have a high acoustic backscatter while the lower 10 to 18 m are transparent and do not reveal any layering.

#### Eurasian Basin

The Eurasia Basin contains an axial mid-oceanic spreading ridge (Gakkel Ridge), which divides it into two smaller sub-basins: the Eurasia-faced Nansen Basin and the Lomonosov-faced Amundsen Basin. All these morphostructural provinces were crossed as RV POLARSTERN moved north-westward from 82°55' N, 28°50' E to 88°37' N, 47°21' E (Fig. 12).

The Nansen Basin has a very flat sea-floor. The continuous PARASOUND record over the entire basin is slightly disturbed by ice-caused noise. The signal penetration is up to 50 m below the sea-floor.

A debris flow facies extends from the Barents continental margin upon the nearest parts of the basin up to about 83°23' N, 28°16' E. It is well-distinguished due to high reflective acoustic characteristics and the clear absence of stratified internal structure. Toward the internal part of the basin, these sediments are gradually replaced by a facially different type of a pronounced layered sedimentary succession (App 5). The seismograms show, that it contains up to 7 individual rhythms which are highly reflective at their upper parts and transparent at the lower ones. We tentatively suggest this succession to be composed of distal turbidites.

On the acoustic record given in App. 5 one can see a slight but rather clear uplifting affecting the lower strata. The thickness of the rhythms is two time smaller than those at both sides of the uplift. This is evidence of growing of the uplift simultaneously with sediment accumulation. We consider this phenomena as an initial stage of mud diapirism which is well-developed northerly. App. 6 shows three diapirs which are in different stages of growing. The middle one, which appears to be the oldest, arises up to 30 m above the sea-floor. These diapirs have acoustically transparent cores similarly to mud-cored diapirs known from other regions (Niessen and Musatov, 1997). These features suggest that the succession of the distal turbidites in the Nansen Basin may be underlain by a mud-rich sequence of an unknown age.

The Gakkel Ridge was crossed between 84°59' N, 24°52' E and 86°27' N, 10°21' E. The PARASOUND section is characterised by a very poor record that is obviously a result of a complicated morphology of the ridge. In a few cases the seismograms contain short fragments of readable records where one can recognise some meters to 30 m thick sedimentary successions mostly occurring within local depressions (App. 7). However, such a fragmented record does not allow tracing neither the morphological features of the Gakkel Ridge nor the facial peculiarities of the sub-bottom sediments.

The Amundsen Basin is represented by a very flat deep-water plain whose major part lies at about 4.380 m. As compared to the Nansen Basin, here we have reduced signal penetration (10 - 30 m) and more ice-caused noise. Nevertheless, the acoustic record revealed a pattern which is very similar to what we observed in the Nansen Basin. The debris flow facies is predominant along the Gakkel-faced part of the section (App. 8) while the opposite part of the section contains a mostly well-stratified succession suggesting to be composed of distal turbidites.

#### Lomonosov Ridge

We crossed the Lomonosov Ridge twice: in its western Canadian part and in the eastern Siberian one (Fig. 12).

The western Lomonosov Ridge between 88°37' N, 47°21' W and 88°00' N, 101°07' W is characterised by a very poor PARASOUND record greatly disturbed by noise and loss of the signal due to the complex morphology of the ridge. Two examples of the



seismograms (App. 9 and App. 10) show a difference in sedimentary pattern in the Eurasia-faced slope area of the ridge (App. 9) and in its crestal part (App. 10) where the relief becomes smoother.

The Siberia-faced segment of the ridge was studied between 84°36.5' N, 160°27.6' E and 79°56.6' N, 142°07.6' E. Generally this part of the ridge reveals some asymmetry of its morphology with a very steep escarpment-bounded western flank and a more gentle eastern slope. The ship track mostly ran along the crest of the ridge where the water depth varies little and the topography is not as complicated as along both flanks of the ridge. Moreover, the whole ridge was crossed once on a W to E directed profile from the start point at 81°30' N, 138°02' E to the end point at 81°29.3' N, 146°27.4' E. Thus, the recorded PARASOUND data have different quality (Table 5) which generally depends on the relief character since the ice conditions were easier than in the Alpha Ridge area.

The majority of the recorded seismograms revealed the occurrence of well-stratified sediments with total penetrated thicknesses varying from 10 to 100 m. App. 11 gives an example from the crest of the ridge covered by a 40 m thick sedimentary sequence. Due to differences in the acoustic imaging and the presence of strong reflectors, it can be divided into three individual units. The two upper units are comparable to those reported by Niessen and Musatov (1997) southerly, where the internal structure of the penetrated sedimentary cover becomes more pronounced. These three units are typical for most of the crossed part of the ridge. However, in some cases another remarkable transparent unit "B" occurs between units "A" and "C". Over most of the crossed area this unit is lacking being truncated by Unit "A" (App. 12). This gives evidence of a distinct unconformity at the bottom of Unit "A" which can be the result of a regional tectonic and/or paleoceanographic event.

Generally one can point out that sediment thickness increases from north to the south approaching the Siberian continental margin. This appears to be related to increasing sediment supply by the large Siberian rivers. App. 13 illustrates the occurrence of a more than 100 m thick sedimentary sequence at geological station PS 051/058 which is located in the area of the western escarpment of the ridge. Here, an approx. 100 m step in sediment can be found. It might have been created by a slope instability.

#### Makarov Basin

The Makarov Basin separates the Alpha and Lomonosov ridges. It was also crossed twice in its western and eastern parts whose acoustic characteristics are quite different.

The western Makarov Basin is divided into two depressions by a very narrow positive feature called Marvin Spur (Fig. 12). The PARASOUND record obtained here is of poor and very poor quality mostly because of the great noise produced by breaking of the heavy ice. Also in the area of the Marvin Spur we failed to find a real signal because of steep slopes. Thus, we illustrate this part of the Makarov Basin

with three fragments of the acoustic record obtained from those parts of the basin which are occupied by deep water plains.

The depression between the Lomonosov Ridge and Marvin Spur revealed about 20 m of penetrated sediments. This succession has an acoustic pattern very similar to those of the Amundsen Basin (App. 14). The central part of this depression contains a twenty-meters-high hill which has the same acoustic expression as the hills found in the Nansen Basin. It is a symmetrical cone-shaped feature with an acoustically transparent core. We suggest it to be the result of mud diapirism, but a possible connection to the gas releasing process has also to be taken into account.

Another depression between the Marvin Spur and Alpha Ridge is filled with well-stratified sub-bottom sediments with a thickness up to 50 m (App. 15 and App. 16). This sequence rests on a transparent acoustic unit. The interface between these units is represented by a very clear unconformity of unknown age. We found this unconformity in two areas within this part of the Makarov Basin (App. 15 and App. 16). This may be evidence of a, to some extent, regional character of this unconformity.

The eastern Makarov Basin was crossed in an area between 84°52.4' N, 171°48.0' E and 84°36.5' N, 160°27.6' E (Fig. 12). Morphologically this part of the basin is simpler. It contains a flat sea-floor which lies generally below 3.400 m of water depth. The PARASOUND data are of good quality with the penetration up to 50 m. App. 17 represents a typical example of the obtained record showing an undisturbed sedimentary sequence characterised by very thin layering. This sequence may be composed of sediments produced by gravity flows from the adjacent East Siberian continental margin.

#### Alpha Ridge

In this cruise we were able to reach the western part of the Alpha Ridge topped by the Lyon Sea Mount (Fig. 12). The operations in this area were carried out in extremely heavy ice conditions that resulted in considerable PARASOUND data signal loss. Especially poor data are characteristic for the northern slopes of the ridge (DESO 7, 9 and 10, Fig. 12) whose topography is much more complicated than it is shown on the existing maps. The crestal part of the ridge is the only area where the quality of the record allows to follow some peculiarities of the sub-bottom sediments (App. 18 and App. 19). As consistent with these data, the penetrated sedimentary cover has more or less the same acoustic pattern in different parts of the Lyon Sea Mount and is represented by stratified sediments. The penetration is in the range of 5 to 20 m and becomes reduced on sea-bottom highs.

### 3.2 Geological sampling, description, and methods applied aboard RV POLARSTERN

#### 3.2.1 Aerosol sampling and size-distribution measurements (V. Shevchenko)

Sampling of aerosols for elemental analysis was carried out aboard RV POLARSTERN approximately 20 m above sea level by pumping of air through Filtrak-388 filters (D= 47 mm; air flow about 10 m<sup>3</sup> per hour). To exclude contamination from the ship, sampling was interrupted when the relative wind direction was not opposite to the ship heading. No samples were collected during rain and snow. During the expedition 3 samples were collected (Table 6). Elemental composition will be studied in Moscow by Instrumental Neutron-Activation Analysis (INAA).

Measurements of aerosol size distribution of particles larger than 0.5 µm were carried out at 61 sites (Table 7) using PC-218 photoelectrical particle counter (Royco, USA). In each series, 3 parallel measurements of particle concentrations in the ranges of 0.5 - 1, 1 - 2, 2 - 3, 3 - 5, and 5 - 10 µm were done. Aerosol size distribution of particles in the range from 0.005 µm to 1 µm were measured by DAES-3 electrostatic particle counter (Table 8).

#### 3.2.2 Sampling of snow, melt-water ponds, and dirty sea ice (V. Shevchenko)

Aeolian transport of particulate matter onto Arctic sea ice is one source of sedimentary material in the Arctic. The annual deposition rates from eolian transport on the Central Arctic ice cover, however, are estimated to be very low to account for the high sediment loads observed in the Eurasian Basin (Pfirman et al., 1990). But atmospheric deposition of any individual components onto the Central Arctic ice surface practically has not been studied yet. In order to estimate contents of some constituents we carried out sampling of snow.

Snow and water from melt ponds samples were collected for chemical composition studies. Sampling was carried out using helicopter. Date and position of sampling are listed in the Table 9. On ice-floes samples of the upper 2 cm layer of snow and water from melt ponds were collected for chemical analysis (macrocomponents and trace elements). For sampling we used precleaned class 100 bottles, a plastic shovel, and plastic bags. Samples were stored in the refrigerator at -30 °C until processing in home laboratories. Ion chromatography and atomic absorption spectrophotometry will be carried out at AWI Bremerhaven (M. Kriews). Other subsamples will be melted and filtered through preweighted Whatman GF/F and Nuclepore filters to calculate concentrations of total suspended matter, particulate organic carbon, particulate organic nitrogen, and to determine contents and species composition of biogenic particles. It is also planned to study biomarkers and C-13 isotope

Tab. 6: List of samples of aerosol collected by filtration.

No.	Date-time (UTC)	Coordinates beginning/end	
		Latitude	Longitude
1	beginning/end		
	02.07-05.20	71°53.2'N	22°37.3'E
	02.07-11.20	72°38.9'N	25°01.0'E
	02.07-12.00	72°43.5'N	25°15.3'E
	02.07-18.40	73°30.1'N	27°50.3'E
	02.07-19.10	73°33.8'N	28°02.5'E
	02.07-22.10	73°54.9'N	29°14.5'E
2	04.07-05.10	76°15.0'N	35°50.2'E
	04.07-10.10	77°03.0'N	36°44.0'E
	04.07-12.30	77°25.1'N	37°28.2'E
	04.07-12.50	77°27.9'N	37°39.5'E
	04.07-14.20	77°40.7'N	38°40.3'E
	04.07-17.25	78°14.5'N	40°20.5'E
	05.07-04.40	80°08.6'N	40°35.3'E
	05.07-11.35	81°00.0'N	37°38.3'E
	05.07-12.40	81°08.9'N	36°59.1'E
	05.07-14.40	81°22.3'N	37°15.1'E
05.07-15.05	81°24.0'N	37°11.0'E	
05.07-18.45	81°30.6'N	34°49.6'E	
3	13.07-05.25	87°08.2'N	139°37.1'W
	13.07-08.05	86°56.3'N	144°03.2'W
	13.07-09.25	86°50.7'N	144°20.8'W
	13.07-11.25	86°42.8'N	146°22.4'W
	13.07-12.20	86°39.0'N	146°56.3'W
13.07-13.30	86°33.4'N	147°38.7'W	

Tab. 7: Time and locations of aerosol size distribution measurements by PC-218 (Royco, USA) particle counter

NN	Date, time (UTC)	Coordinates	
		Latitude	Longitude
1	30.06-08.00	66°21.4'N	9°35.4'E
2	30.06-09.30	66°33.6'N	9°51.2'E
3	30.06-12.30	67°00.7'N	10°27.0'E
4	30.06-14.10	67°10.8'N	10°40.6'E
5	30.06-16.25	67°29.9'N	11°07.6'E
6	30.06-20.30	67°59.9'N	12°04.8'E
7	01.07-05.40	69°11.6'N	14°34.0'E
8	01.07-09.07	69°34.5'N	15°43.2'E
9	01.07-10.00	69°40.9'N	16°02.0'E
10	01.07-12.35	69°57.5'N	16°52.0'E
11	01.07-16.50	70°17.8'N	17°55.7'E
12	02.07-04.20	71°45.0'N	22°13.1'E
13	02.07-06.12	72°00.0'N	22°56.5'E
14	02.07-10.10	72°30.7'N	24°35.4'E
15	02.07-12.15	72°45.3'N	25°21.2'E
16	02.07-14.25	73°00.1'N	26°10.3'E
17	02.07-18.40	73°30.1'N	27°50.3'E
18	02.07-19.10	73°33.8'N	28°02.5'E
19	02.07-22.10	73°54.9'N	29°14.5'E
20	04.07-04.25	76°05.7'N	35°44.4'E
21	04.07-05.10	76°15.0'N	35°50.2'E
22	04.07-07.28	76°41.1'N	35°42.5'E
23	04.07-10.10	77°03.0'N	36°44.0'E
24	04.07-13.04	77°30.0'N	37°48.2'E
25	04.07-16.14	78°01.9'N	39°41.7'E
26	04.07-22.15	79°06.2'N	40°30.5'E
27	05.07-04.40	80°08.6'N	40°35.5'E
28	05.07-07.23	80°36.2'N	39°22.3'E
29	05.07-11.35	81°00.0'N	81°00.0'E
30	05.07-15.05	81°24.0'N	37°11.0'E
31	05.07-18.45	81°30.6'N	34°49.6'E
32	06.07-00.10	81°58.9'N	34°42.0'E
33	06.07-08.53	82°15.0'N	34°50.0'E
34	06.07-17.45	82°49.7'N	31°52.8'E
35	07.07-05.15	83°26.8'N	27°23.2'E
36	07.07-17.15	84°20.0'N	25°55.0'E
37	12.07-20.45	87°31.1'N	130°45.8'W
38	12.07-22.40	87°26.8'N	136°02.0'W
39	13.07-05.25	87°08.2'N	139°37.1'W

Tab. 7 (continuation)

NN	Date, time (UTC)	Coordinates	
40	13.07-06.35	87°01.3'N	141°35.7'W
41	13.07-09.25	86°50.7'N	144°20.8'W
42	16.07-10.45	85°08.0'N	171°25.9'W
43	17.07-10.15	85°30.7'N	174°16.5'W
44	18.07-18.05	85°45.7'N	177°55.3'W
45	19.07-08.30	85°22.1'N	177°35.7'E
46	19.07-15.10	85°03.5'N	176°01.1'E
47	19.07-21.43	84°50.1'N	169°59.0'E
48	20.07-05.25	84°39.6'N	161°37.5'E
49	20.07-06.55	84°34.2'N	160°00.0'E
50	20.07-16.30	84°33.5'N	149°58.7'E
51	21.07-04.50	83°51.8'N	146°22.5'E
52	21.07-14.30	83°30.0'N	144°19.0'E
53	21.07-17.45	83°15.6'N	142°23.0'E
54	21.07-19.45	83°00.7'N	142°08.9'E
55	22.07-07.45	82°00.1'N	141°51.9'E
56	22.07-09.00	81°52.1'N	141°43.6'E
57	22.07-14.25	81°48.3'N	137°56.1'E
58	23.07-21.45	81°00.0'N	142°58.5'E
59	24.07-05.55	80°13.5'N	142°57.3'E
60	24.07-08.15	80°00.4'N	142°22.3'E
61	24.07-09.10	79°56.4'N	142°07.2'E

Tab. 8: Time and locations of aerosol size distribution measurements by DAES-3 electrostatic particle counter

NN	Date - time (UTC)	Coordinates	
		Latitude	Longitude
1	30.06-14.10	67°10.9'N	10°40.6'E
2	01.07-09.40	69°38.5'N	15°55.0'E
3	01.07-10.00	69°40.9'N	16°02.0'E
4	01.07-12.00	69°54.8'N	69°54.8'E
5	02.07-05.20	71°53.2'N	22°37.3'E
6	02.07-06.00	71°58.8'N	22°53.1'E
7	02.07-06.12	72°00.0'N	22°56.7'E
8	02.07-08.16	72°16.5'N	23°46.9'E
9	02.07-15.30	73°07.7'N	26°34.2'E
10	02.07-17.50	73°18.9'N	27°12.8'E
11	02.07-18.40	73°30.1'N	27°50.3'E
12	04.07-05.10	76°15.0'N	35°50.2'N
13	13.07-06.35	87°01.3'N	141°35.7'W

Tab. 9: Time and locations of sampling of snow, melt water ponds, and sea ice

Date	Sampler	Floe	Latitude (N)	Longitude	Snow	Water	Sea ice
06.07.1998	Shevchenko	1	82°21.27 N	33°51.18 E	1		
		2	82°21.33 N	33°20.65 E		1	
		3	82°29.18 N	33°39.34 E			2
07.07.1998	Shevchenko	4	83°33.18 N	27°14.76 E	2	3	
		5	83°37.84 N	26°54.88 E	3		
		6	83°39.52 N	27°01.24 E		4	
		7	83°54.52 N	25°51.78 E	4	5	
		8	83°58.52 N	25°31.22 E		6	
		9	84°00.10 N	25°19.10 E			
08.07.1998	Shevchenko	10	85°53.36 N	15°56.54 E	5	7	1+2
		11	86°04.10 N	14°54.39 E		8	3+4
		12	86°39.46 N	7°41.41 E			5+6
		13	86°51.70 N	7°52.00 E		9	7
10.07.1998	Müller	14	86°51.63 N	6°43.56 E	6		
		15	88°04.40 N	89°53.23 W	7	10	8
		16	88°02.19 N	100°56.56 W	8	11	9
12.07.1998	Polozek	17	87°59.06 N	100°44.69 W	9	12	10
		18	87°33.39 N	115°33.46 W	10	13	
		19	87°34.30 N	115°05.64 W			11
13.07.1998	Hefer	20	87°34.65 N	116°36.35 W	11		12
		21	87°29.94 N	119°25.13 W			13
		22	87°31.20 N	118°49.48 W			14
		23	86°59.54 N	143°22.71 W	12	14	
		24	86°59.54 N	143°22.71 W			15
		25	86°57.41 N	144°14.81 W	13		
14.07.1998	Rödle	26	86°37.45 N	147°08.55 W	14	15	16
		27	86°33.09 N	148°03.64 W	15		
		28	86°32.43 N	147°14.40 W	16		17
15.07.1998	Usbeck	29	86°25.36 N	148°19.85 W	17	16	
		30	86°22.38 N	148°28.66 W			18
		31	86°23.15 N	149°31.45 W	18		
16.07.1998	Drachev	32	85°21.86 N	155°23.49 W	19	17	
		33	85°24.03 N	155°41.28 W	20		19
17.07.1998	Golikov	34	85°09.07 N	171°20.46 W	21	18	
		35	85°10.35 N	171°29.50 W			20
18.07.1998	Yoon	36	85°29.70 N	174°44.44 W	22	19	21
		37	85°35.68 N	173°43.74 W	23		
		38	85°37.01 N	174°05.21 W	24		
18.07.1998	Sokolov	39	85°45.14 N	177°01.22 W	25	20	
		40	85°43.24 N	178°43.21 W			22
19.07.1998	Musatov	41	85°40.40 N	176°56.23 W	26		23
		42	85°39.19 N	177°51.71 W			24+25
21.07.1998	Rödle	43	85°21.04 N	177°43.80 E	27	21	26
		44	85°13.90 N	178°26.70 E	28		
		45	83°31.00 N	144°46.59 E	29	22	
22.07.1998	Norgaard-Pedersen	46	83°33.57 N	144°58.95 E	30	23	27
		47	83°33.29 N	144°49.77 E	31		
		48	81°52.59 N	141°36.00 E	32	24	
		49	81°48.69 N	141°44.90 E	33		
23.07.1998	Matthiessen	50	81°51.19 N	141°16.87 E	34		
		51	81°26.05 N	142°32.32 E	35		
		52	81°31.50 N	141°50.59 E	36		
23.07.1998	Müller	53	81°33.50 N	141°44.77 E	37	25	
		54	81°36.06 N	142°17.85 E			28
		55	81°28.40 N	145°03.88 E	38	26	29
		56	81°28.40 N	145°03.88 E			
		57	81°28.86 N	145°25.92 E	39		



composition in these samples. The obtained data will be used for the estimation of deposition of chemical components to the Arctic Ocean surface from the atmosphere. Later scanning electron microscopy with X-ray micro analysis will be carried out to study the composition of individual particles. The studies of composition of particulate matter contained in snow are to be carried out at AWI Bremerhaven, IORAS Moscow, and University of Antwerpen.

Sediment transport via sea ice is expected to contribute significantly to deep-sea sedimentation at least in regions of ice ablation (Pfirman et al., 1990; Nürnberg et al., 1994). It is important to study the role of different sources in supplying the Central Arctic, especially the Alpha Rigde area, with ice-rafted sediments. Thus, "dirty sea ice" has been samples at numerous locations during the ARK-XIV/1a Expedition (Table 9). At AWI the "dirty ice" samples will be melted and filtered. After that grain size analyses, mineral and elemental composition, contents of organic compounds, isotope composition of C species composition of algae will be studied at AWI, IORAS and MMBI. Using the obtained data we try to estimate the input of matter from different source regions delivered in the study area by the Transpolar Drift or Beaufort Gyre systems.

### 3.2.3 Sampling in the water column using sediment traps (V. Shevchenko)

In order to elucidate the contribution of ice-derived mineral and organic material to particle flux rates, sedimenting material was collected by short-term deployments of sediment traps attached to the ice floes. The sediment traps were deployed by hand over the edge of ice floes, at a distance of at least 200 m away from the ship (Table 10). Helicopter was used to bring people and equipment onto the ice floes. Deployments consisted of two single traps (D= 12 cm) positioned at 50 and 75 m of water depth. The traps are fitted with a baffler at the top. The sampling bottles were filled with prefiltered sea water to which NaCl was added to increase the density (to salinity of about 40 ‰). The solution was poisoned with HgCl<sub>2</sub> prior and after the deployment. Samples collected by sediment traps will be analyzed for particulate organic carbon, particulate organic nitrogen, Chl-a and seston content. Light and scanning electron microscopic analyses will also be performed. At the same stations water samples for microalgae studies were taken from the sea surface (0 m) manually from the edge of ice floes and from the 25, 50 and 75 m depths from the rosette Niskin bottles. Aggregates (colonies) of diatoms were collected from the edge of ice floes where sediment traps were deployed. The trap data, combined with related data from the water column, will allow quantitative and qualitative evaluations of daily vertical particle flux rates.

Tab. 10: Sediment trap deployments; phytoplankton (0, 25, 50 and 75 m depths) and ice flora (0 m) sampling.

Station No.	Date	Position		Duration (hr)	Quantity of ice flora samples
		Latitude	Longitude		
51/034	15.07	85°22.3'N	155°25.2'W	6	4
51/038	16.07	85°08.0'N	171°25.6'W	3	3
51/046	18.08	85°45.1'N	177°00.5'W	6.25	4

3.2.4 Sea floor sediment sampling and description  
(K. Fahl, J. Hefter, H. Kassens, N. Koukina, J. Matthiessen, C. Müller, E. Musatov, J. Mutterlose, N. Nørgaard-Petersen, K. Polozek, and R. Stein)

#### Sampling of Near-Surface Sediments

Surface sediments were taken routinely at almost all geological stations (Fig. 11) with the giant box corer (GKG; 50 x 50 x 60 cm). The surface sediments of the GKG were sampled for sedimentological, micropaleontological, and geochemical investigations. In addition, three plastic tubes (12 cm in diameter) and one plastic box (cross section of 7.5 x 15) covering the entire sediment column gained by GKG were taken for sedimentological, geochemical, and stable isotope investigations, and for archiving at AWI.

At several stations (see station list), the AWI multicorer ("MUC"; manufactured by Fa. Wuttke, Henstedt-Ulzburg) with 12 tubes of 6 cm in diameter was used. The penetration weight of the MUC is 250 kg.

#### Coring and Sampling of Long Sediment Cores

The gravity corer (SL) and the kastenlot corer (KAL) were used to obtain long sediment cores. The gravity corer has a penetration weight of 1.5 t, and a core barrel segment length of 5 m with a diameter of 120 mm. The core barrels used during ARK-XIV/1a had lengths of 5 and 10 m. The length of the obtained cores vary between 0 and 635 cm (Fig. 13). The kastenlot (Kögler, 1963), a gravity corer with a rectangular cross section of 30 x 30 cm, has a penetration weight of 3.5 t and a corebox segment sized 30 x 30 x 575 cm (manufactured by Hydrowerkstätten Kiel). The length of the box core boxes used was 11.75 m plus about 30 cm for the core catcher. The great advantage of this kastenlot is the wall-thickness of only 0.2 cm. Because of the great cross-sectional area (900 cm<sup>2</sup>) and the small thickness of the walls, the quality of the core was generally excellent. The length of the obtained core was 719 cm (PS51/038-4) (Fig. 13).

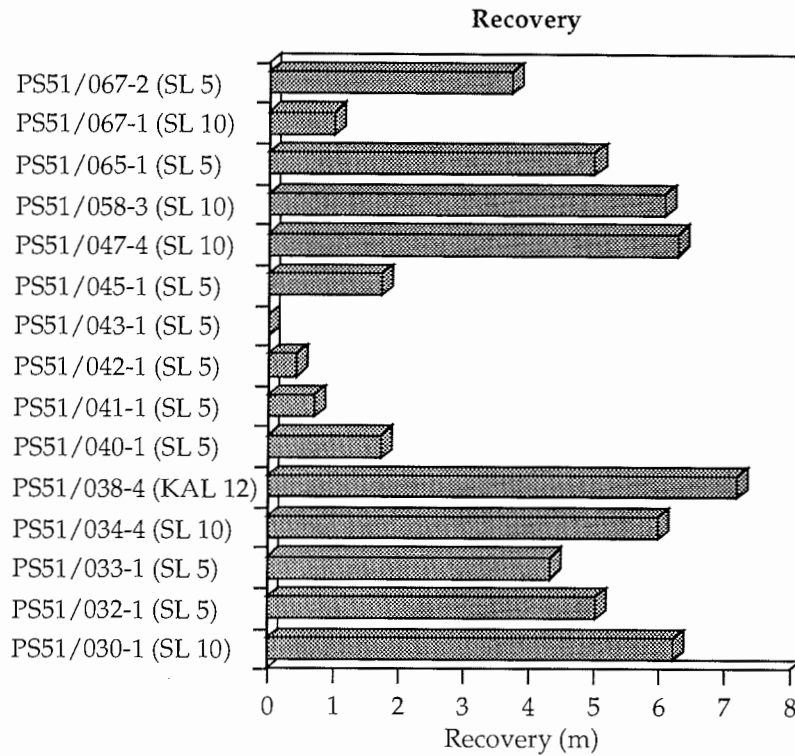


Fig. 13: Recovery of kastenlot (KAL) and gravity (SL) cores.

Six of the gravity cores were opened, described, and sampled for smear-slide analysis onboard POLARSTERN. Before opening of the SL cores, core logging was performed (see chapter 3.3.1). Sampling of SL cores will be performed onshore for stratigraphical, sedimentological, geochemical, and micropaleontological studies (AMS<sup>14</sup>C dating, stable isotopes, grain size, mineral composition, major and minor elements, carbonate, organic carbon, biomarker, microfossil assemblages, etc.).

Sampling of the KAL core for the same investigations was performed as follows: three plastic boxes (100 x 16 x 7.5 cm) covering the entire core (AWI Archive; AWI geochemistry, sedimentology, mineralogy, and stable isotopes; GEOMAR sedimentology and stable isotopes). One plastic box (100 x 9 x 7.5 cm) covering the entire core was taken for core logging and afterwards deep-frozen at -30°C for organic-geochemical studies to be later performed at the home laboratory. In addition, single samples were taken from the entire core for specific mineralogical and micropaleontological studies (IORAS Moscow, VNIIO St. Petersburg, MMBI Murmansk).

## Sediment Description and Characterization

- Visual core description

The sediment cores were routinely photographed and described, and are graphically displayed within the annex. Sediment colors were identified according to the "Munsell Soil Color Chart".

- Smear slide investigations

Smear-slide investigations were performed to obtain estimates of the grain size and sediment composition (i. e., biogenic and terrigenous components) and for the classification of the sediment type (e. g., silty clay, sandy silt, etc.).

- Radiographs

Sediment slabs of 0.5 cm in thickness were taken continuously from KAL and all opened SL cores. X-ray images has been produced onboard POLARSTERN in order to elucidate sedimentary and biogenic structures and to determine the number of coarse-grained detritus >2 mm for evaluation of the contents of ice-rafted debris (IRD; cf., Fig. 21) (for method see Grobe, 1987).

### 3.3 Physical properties in marine sediments

During ARK-XIV/1a physical properties were determined on whole cores by logging (magnetic susceptibility, P-wave velocity, wet bulk density and porosity) and on discrete samples after core opening (wet bulk density, water content, porosity). Physical properties of marine sediments are important parameters for the interpretation of the sedimentary record. These data allow to enhance the paleoceanographic interpretation of each site (e. g. to determine sediment accumulation rates) and to provide data for lateral core correlation and stratigraphic control. Furthermore, the magnetic susceptibility which is defined as the dimensionless proportional factor of an applied magnetic field in relation to the magnetization in the sample, can be used as an indicator for marine versus terrestrial origin of the sediments (e. g., Nowaczyk, 1991). In addition, P-wave velocity and wet bulk density are basic parameters for the calculation of synthetic seismograms in order to compare the cored sedimentary record with high resolution seismic profiles obtained with the PARASOUND system.

#### 3.3.1 Continuous whole-core logging of wet bulk density, P-wave velocity and magnetic susceptibility (R. Stein, R. Usbeck and K. Polozek)

Wet Bulk Density (WBD) and P-wave velocity and magnetic susceptibility were measured in 1-cm intervals on gravity and kastenlot cores taken during the cruise. We have used the "Multi Sensor Core Logger (MSCL-14)", manufactured by Geotek (UK), which allows the determination of core diameter, P-wave travel time, gamma-

ray attenuation and magnetic susceptibility. The system is automated (PC based) and designed for non-destructive logging of up to 1.3 m long whole-core sections. In case of kastenlot cores, polystyrene boxes (size inside 82.5 x 72 x 1000 mm) were logged which were previously filled with sediments by pushing the boxes into the cores shortly after the kastenlot was opened. Because the loop sensor used has a different response to varying core diameter, all magnetic susceptibility values determined for kastenlot boxes are multiplied by 0.82 (Table 11) according to the manufacturer's correction instructions. The data is expressed in SI-units, although no correct volume susceptibility can be assessed due to the loop sensor geometry.

A detailed description of the MSCL system is given by Kuhn (1995), its calibration is described by Niessen (1997) and Weber et al. (1997). The characteristics are summarized in Table 11. During the time of the cruise the gamma ray attenuation was calibrated to density using aluminum, graphite and water. The raw data was processed using the Geotek Software Version 3.0. Additionally, a Kaleidagraph Macro was improved during the cruise in order to calculate the correction for count rate effects on the attenuated gamma data as described in Weber et al. (1997).

For all sediment cores logged aboard RV POLARSTERN during the ARK-XIX/1a Expedition, the records of porosity, WBD and magnetic susceptibility are listed in the Appendix. The porosity values have been calculated from the measured WBD and a grain density of  $2.65 \text{ g cm}^{-3}$  (Weber et al., 1997). As an example, the data of Kastanlot Core PS51/038-4 are shown in Figure 14. All three variables show rhythmic/cyclic variations with changing amplitudes, suggesting changes in sediment composition and/or grain size (cf., Chapter 3.5). In general, the WBD values calculated from the MSCL correlate with those determined on discrete samples. There is a similar trend, although the MSCL densities are mostly lower than those of discrete samples (Fig. 14). Based on the porosity and WBD records, the sedimentary sequence can be divided in three intervals. Interval I (445 cmbsf to bottom of core) is characterized by porosity and WBD values ranging between 50 and 70 % and between  $1.55$  and  $1.8 \text{ g cm}^{-3}$ , respectively. Interval II (250 to 445 cmbsf) is characterized by low-amplitude variations in porosity and WBD ( $60 - 65\%$  and  $1.58 - 1.68 \text{ g cm}^{-3}$ ). In the upper 250 cmbsf (Interval III) the amplitude of both parameters distinctly increases, reaching a maximum range in the uppermost 150 cmbsf. The increase in magnetic susceptibility at about 350 cmbsf coincides with increased occurrence of IRD (cf., Fig. 21) and a change in the grey scale record (cf., Fig. 16).

Based on whole-core logging records, a lateral correlation between sediment cores is possible as shown for the Alpha-Ridge Transect PS51/030-1 to PS51/034-4 (Fig. 15 a and b). The WBD records of all four cores (Fig. 15 a) display a similar very prominent pattern. The lower part of the records is characterized by WBD values fluctuating around a constant mean values of about  $1.64$  to  $1.68 \text{ g cm}^{-3}$ ; the amplitude is significantly lower than in the upper part. The upper part is characterized by a trend to lower mean values and a distinct increase in the amplitude of fluctuation. At least four major cycles superimposed by shorter-term cycles, are observed in the records (Fig. 15 a). In the magnetic susceptibility records (Fig. 15 b), distinct minimum values

can be correlated in all four cores. Based on the MSCL records, the sedimentation rate of the shallower core PS51/034-4 (water depth 2071 m) appears to be lower (by a factor of about two) than that of the deeper cores from water depths between about 2690 and 2950 m (cf., Chapter 3.5).

Tab. 11: Multi Sensor Core Logger (MSCL-14) specifications

<b>P-wave Velocity and Core Diameter</b>	
Transducer diameter	5 cm
Transmitter pulse frequency	500 kHz
Transmitted pulse repetition rate:	1 kHz
Received pulse resolution	50 ns
P-wave travel-time offset	8.47 $\mu$ s (KAL, 2*3 mm box wall thickness) 7.79 $\mu$ s (SL, 2*2.5 cm liner wall thickness)
<b>Density</b>	
Gamma ray source	Cs-137
Source activity	356 MBq
Source energy	0.662 MeV
Collimator diameter	5 mm
Gamma detector	Scintillation Counter (John Count Scientific Ltd.)
<b>Magnetic Susceptibility</b>	
Loop sensor type	MS-2B (Bartington Ltd.)
Loop sensor diameter	14 cm
Alternating field frequency	0.565 kHz
Magnetic field intensity	approx. 80 A/m RMS
Loop sensor correction coefficient	
SL	2 (113 cm <sup>2</sup> core cross section)
K-rel	
Loop sensor correction coefficient	
KAL	0.82 (59.4 cm <sup>2</sup> box cross section)
K-rel	

PS51/038-4

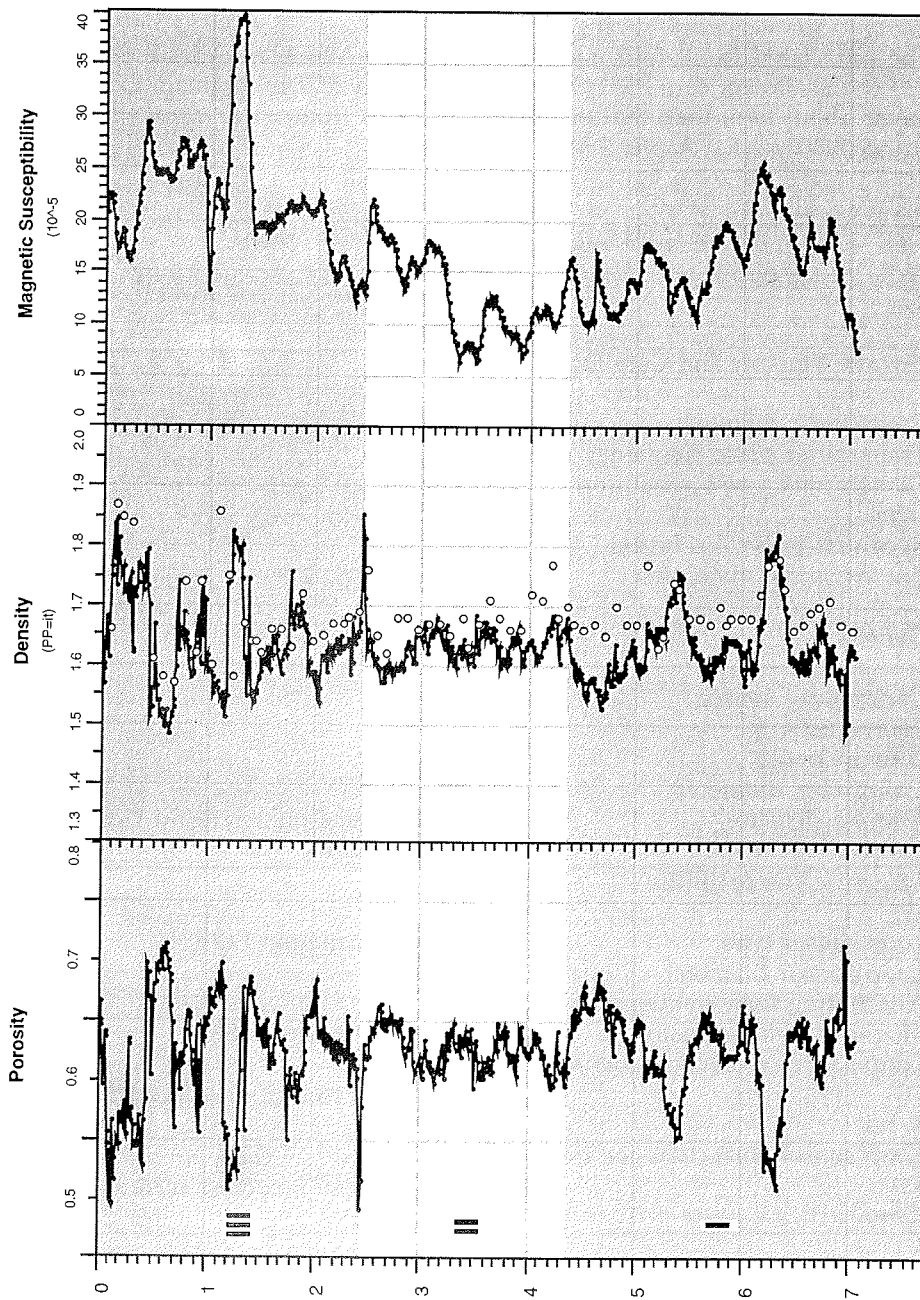


Fig. 14: Porosity, wet bulk density, and magnetic susceptibility records from Kastenlot Core PS51/038-4, obtained by Multi Sensor Logging. Open circles are wet bulk density values measured on discrete samples (cf., Fig. 16).

Density (PP=it)

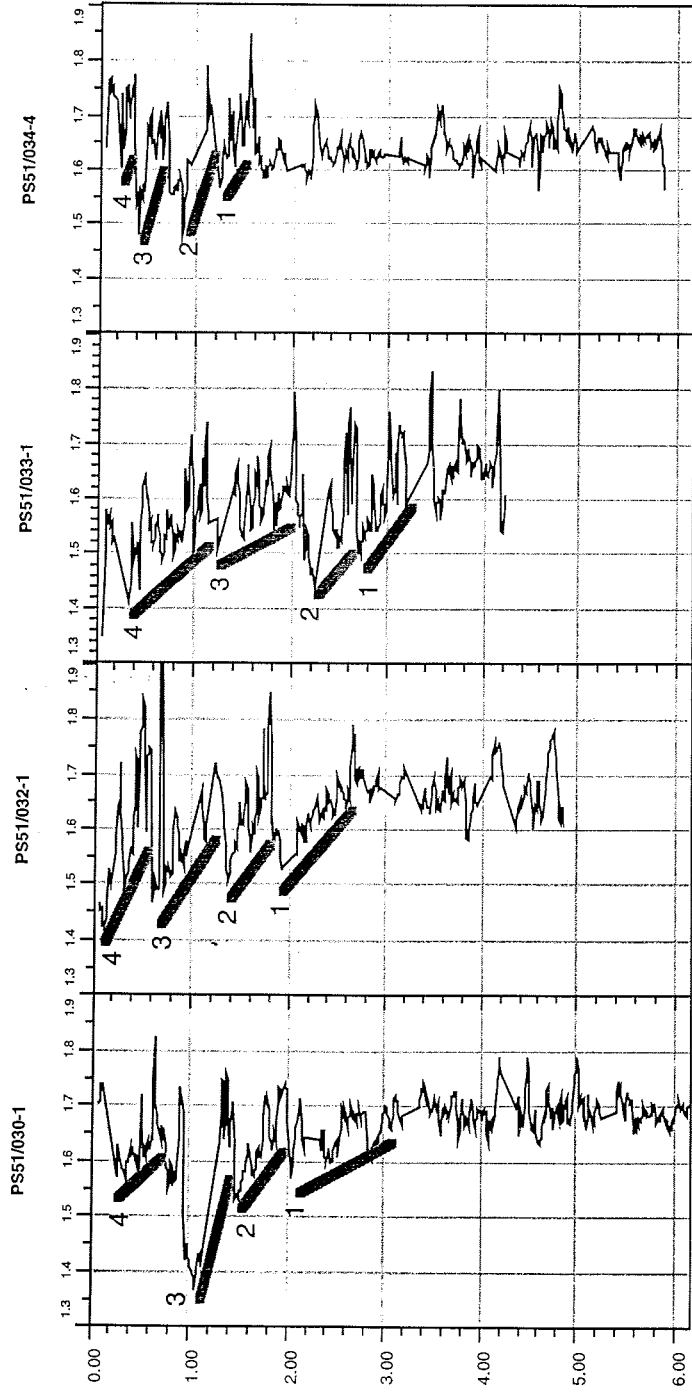


Fig. 15 a: Lateral correlation of whole-core logging results of the Alpha-Ridge-Transect PS51/030-1 to PS51/034-4. (a) wet bulk density records  
Grey-shaded interval of the upper part of the records in (a) and (b) indicates a general change in the pattern of the density records (i. e., decrease in mean value and increase in amplitude of fluctuation).



Susceptibility (10-5)

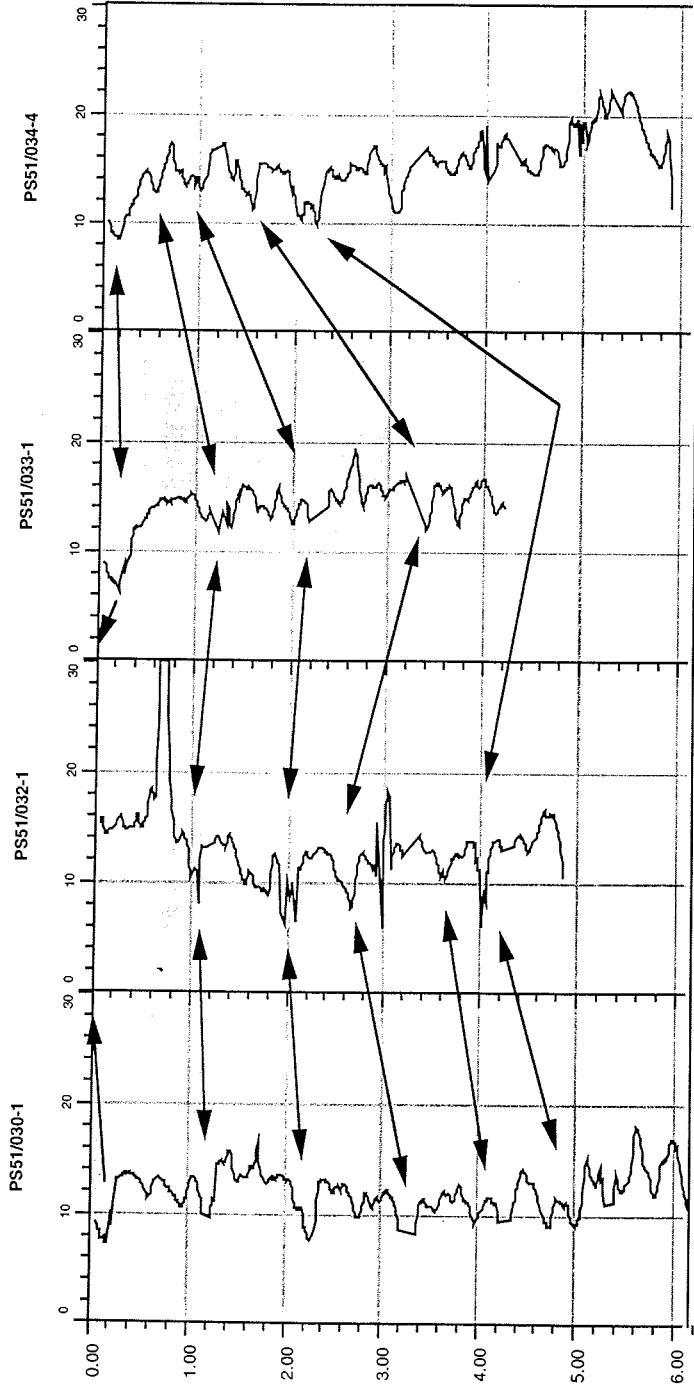


Fig. 15 b: Lateral correlation of whole-core logging results of the Alpha-Ridge-Transect PS51/030-1 to PS51/034-4.  
(b) magnetic susceptibility records  
Grey-shaded interval of the upper part of the records in (a) and (b) indicates a general change in the pattern of the density records (i. e., decrease in mean value and increase in amplitude of fluctuation).

## Alpha Ridge: PS 51/038-4 KAL

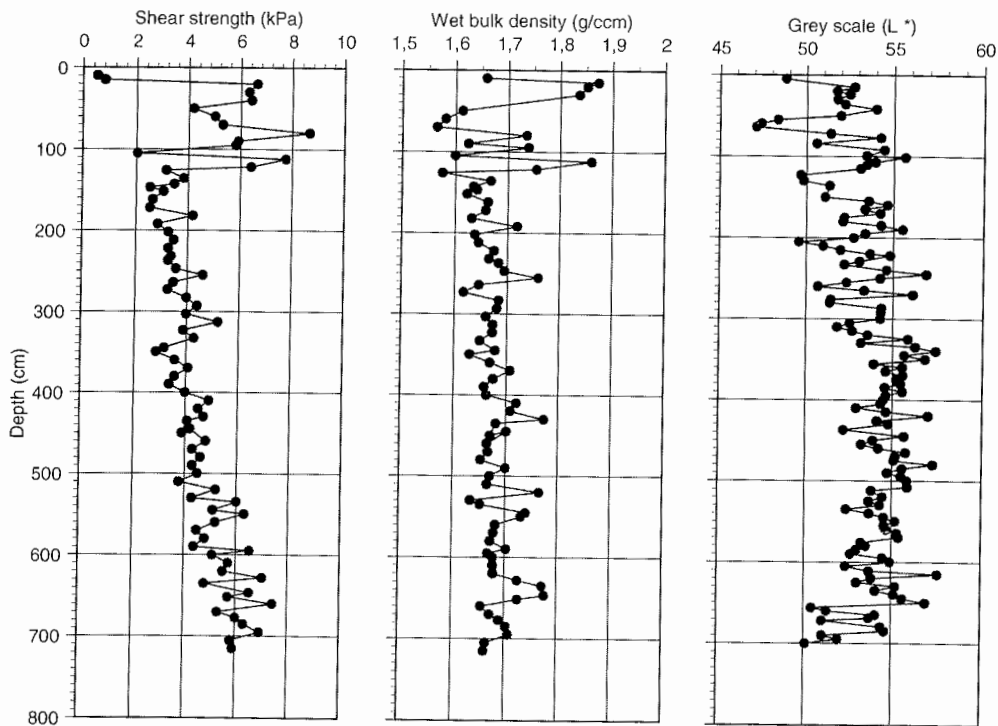


Fig. 16: Physical property record of sediment Core PS 51/038-4 KAL from the ALPHA Ridge at 1473 m water depth.

### 3.3.2. Physical properties of discrete samples (H. Kassens and N. Nørgaard-Petersen)

Sediment physical properties measured aboard on discrete samples included shear strength, index properties (e. g. wet bulk density, water content, porosity), and colour reflectance.

Shear strength: A vane shear instrument (Haake viscometer, RV 3) was used to measure undrained shear strength of undisturbed box and gravity cores (kasten

corer; 30 x 30 x 600 cm). A 20 mm x 8.8 mm vane was used with this instrument, inserted 1 cm deep into the sediment and rotated at a speed of 4 rotations per minute (24°/sec). The measurement interval ranged from 2.5 to 10 cm depending on the down-core variability of sediments. At each depth interval 2 - 4 measurements were taken in order to determine the scatter associated with sediment inhomogeneities, such as bioturbation. Shear strength was measured at peak failure. All values are reported in kPa.

Index properties: From the index properties water content and bulk density, sediment phase relationships as dry density, porosity and void ratio were derived. The index properties were determined from the direct measurement of the total mass of the sample ( $M_t$ ), the dry mass of the sample ( $M_d$ ) and the total volume of the saturated sample ( $V_t$ ). To compensate for ship's motion, mass was determined using a technique of differential counterbalancing on twin top loading electronic balances (Childress and Mickel, 1980). A constant volume sampling tube of 10 ccm was used. The tube was carefully pushed into the sediment, then cut out, trimmed and weighed. After determination of the total (wet) mass and volume, samples were stored for later freeze drying and determination of water content and dry mass in the home laboratory. Wet bulk density ( $M_w$ ) is the density of the total sample, including pore fluid ( $M_w = M_t/V_t$ ). Units are reported in g/ccm. In addition to being one of the most basic measurements for determining material properties, bulk density is also one of the two variables required for calculation of sediment accumulation rates.

Colour reflectance: Colour reflectance was determined directly after core recovery in order to avoid colour changes due to e. g. air contact alteration of the sediments. Measurements were carried out by using the MINOLTA spectrophotometer CM 2002. This system is measuring the spectral reflectance of sediments at wave length from 400 to 700 nm ( $L^* a^* b^*$  colour space; also referred to as the CIELAB space). To average colour inhomogeneities as a result of bioturbation 2 - 3 measurements were taken at each depth interval (field of view 0.8 cm<sup>2</sup>). Lightness, hue, and saturation were registered, whereas only the lightness variable  $L^*$  (grey scale) is reported here.

Preliminary results of Kastenlot Core PS 51/038-4 from the northern slope of the Alpha Ridge at 1.473 m water depth are reported here (Fig. 16):

In general, the uppermost sediment cover (<10 m) on the Alpha Ridge is dominated by Quaternary hemipelagic sediments. The frequency and amplitude variations of the physical property curves represent alternating sediment intervals of silty clay with intervals of sandy silty clay as well as frequent mud clasts-rich units. Sediments show normally consolidated behaviour (e. g. linearly increasing shear strength with depth), with intervals showing deviations from this trend between 20 and 125 cm below sea floor. The deviations can be directly correlated with lithologic changes, such as event deposits of ice-rafted debris and mud clasts (cf., Chapter 3.5), and therefore do not represent past erosional or seabed loading events. From 125 cm to the base of the core at 720 cm below sea floor the shear strength values show a rather

constant downward increase of about 0.5 kPa/m and wet bulk density variations of decreased amplitude. This pattern reflects the rather homogeneous and fine-grained character of the sediments.

The cyclic alternation of yellowish brown (10YR5/4) and dark yellowish brown (10YR4/3) sediment units (cf. core description) seen throughout the core was documented also by colour reflectance measurements. A grey scale record produced (Fig. 16) shows the cyclic character, but reveals also a change in grey scale and cyclic amplitude at about 350 cm below sea floor. This change apparently is not documented by the shear strength and wet bulk density records, but coincides with changes in magnetic susceptibility and IRD content (cf., Figs. 14 and 21, respectively). More investigations are needed to explain the relationship between colour variation and other lithological and physical properties in more detail.

Physical property records of sediment core PS 51/038-4 from the Alpha Ridge correspond to records of sediment core PS 2185-6 from the Lomonosov Ridge at 1052 m water depth (Fütterer, 1992). The high-amplitude physical property pattern observed within the uppermost 125 cm of sediment core PS 51/038-4 correlates well with the pattern observed within the upper 300 cm of sediment core PS 2185-6 from the Lomonosov Ridge (Fig. 17). According to Spielhagen et al. (1997) the Brunhes/Matuyama boundary is at 342 cm below sea floor in the Lomonosov Ridge core. This age correlation also correlates well with the lithostratigraphy (cf., Fig. 22). Thus, sediment accumulation rates during the Late Quaternary seem to have been almost 3 times lower on the Alpha Ridge in comparison to the Lomonosov Ridge.

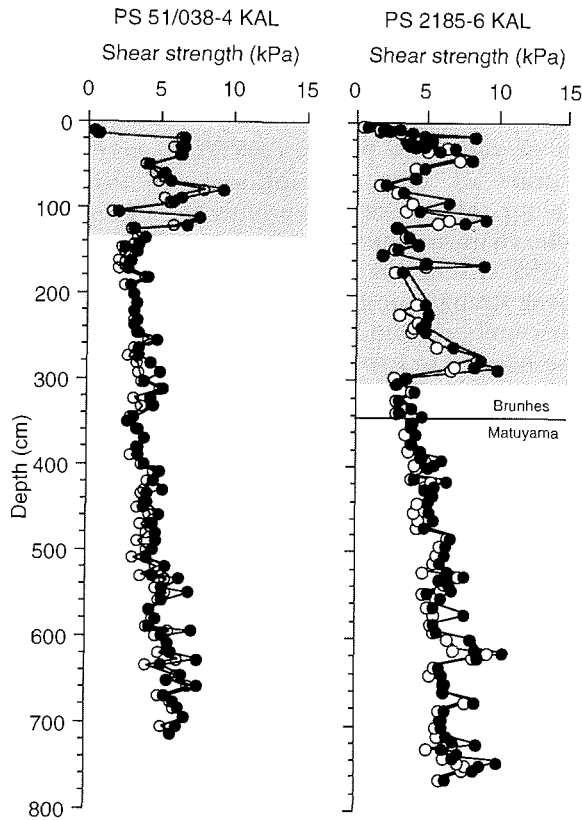


Fig. 17: Shear strength distribution of Alpha Ridge Core PS 51/038-4 and Lomonosov Ridge Core PS 2185-6. Open/solid circles indicate minimum/maximum values. Remarkable is the similarity of both records. Sediment units of different thickness in these two cores are showing comparable shear strength pattern.

#### 3.4. Biostratigraphy (J. Mutterlose and J. Matthiessen)

##### 3.4.1 Material and methods

A total of 127 samples were studied with respect to their micropalaeontological contents. The samples are derived from the following sediment cores: PS51/028 MUC, PS51/029-1 GKG, PS51/030-1 SL, PS51/032-1 SL, PS51/033-1 SL, PS51/034-4 SL, PS51/038-3 GKG, PS51/038-4 KAL, PS51/040-1 SL, PS51/041-1 SL, PS51/067-1 SL and PS51/067-2 SL. For location of the sections compare Table 12.

Tab. 12: List of samples studied for calcareous nannofossils. 1 samples = total of samples studied for each section, 2 nannos " samples yielding calcareous nannofossils, 3 depth = interval from which nannofossils were recovered.

station	1) samples	2) nannos	3) depth
28 - MUC	15	3	22 - 25cm
29-1 GKG	5	3	5 - 30cm
30-1 SL	27	10	30 - 235cm
32-1 SL	3	0	
33-1 SL	6	2	130 - 230cm
34-4 SI	18	2	39 - 77cm
38-3 GKG	5	0	
38-4 KAL	33	4	51 - 151cm
40-1 SL	2	0	
41-1 SL	1	0	
67-1 SL	11	1	40cm
67-2 SL	7	0	

Simple smear-slide preparations were examined under the light microscope using a magnification of 1.500 x. Norland Optical Adhesive was used to attach the cover glasses to the microscope slide. The abundance of microfossils in the material recovered in general is low. Microfossils constitute less than 1 % of the rock, most of the smear slide were made up by quartz, feldspar and mica. One sample (67-2, CC) was disaggregated in hot water and washed over a 63 µm sieve in order to gain foraminifera. However, this sample is barren.

In addition 20 samples were disaggregated and washed over a 21 µm sieve for palynological analyses. Samples, smear slides and residues are housed at the AWI in Bremerhaven.

### 3.4.2 Results

#### Calcareous nannofossils

None of the samples studied yield rich and/or abundant assemblages of calcareous nannofossils. Most of the samples are barren, only 25 of 127 samples contain nannofossils of low diversity. All of the taxa encountered are of Quaternary age: *Gephyrocapsa oceanica*, *Emiliana huxleyi*. The preservation of *Gephyrocapsa* is quite good, in most specimens the oblique bridge is still preserved. More solid coccoliths were observed as well. These, however, can not be assigned to a specific

genus due to fragmentary preservation. Abundance is low as well, coccoliths are extremely rare. In those samples where coccoliths were observed, abundances may be estimated as 1 specimen per 10 fields of view.

Based on the occurrence of *Gephyrocapsa oceanica* the nannofossil bearing strata can be assigned to the nannofossil zones NN 19 - 12 of Martini (1971). Only cores 28 - 1, 24 - 25 cm and 67 - 1, 40 cm yielded definitive specimens of *Emiliana huxleyi*. These samples have latest Pleistocene age and correlate to NN 21.

#### Foraminifera

Rare planktonic foraminifera have been observed, they are, however less common than calcareous nannofossils.

#### Palynomorphs

Only few samples from near-surface sediments washed over 21 µm sieve contained palynomorphs, whereas the smear slides proved to be barren. The low palynomorph recovery may be caused by the strong dilution of residues with coarse silt particles. Processing with hydrofluoric acid is required to further enrich the organic matter. The dark brown silty clays from near-surface sediments contained relatively abundant dinoflagellate cysts, consisting of a monospecific assemblage of *Algidasphaeridium? minutum*. This species is characteristic of relatively low saline cold waters of the high northern latitudes and is in particular common in Holocene sediments.

### 3.5 Lithostratigraphy

(R. Stein, N. Kukina, J. Matthiessen, C. Müller, N. Nørgaard-Petersen and R. Usbeck)

Six long sediment cores with a recovery between 4.5 to 7.2 meters (Fig. 13) were obtained along the northern flank of the western Alpha Ridge (Fig. 11: Cores PS51/030-1, PS51/032-1, PS51/033-1, PS51/034-4, PS51/038-4, PS51/047-4). At the steep slope of a graben-like structure in the westernmost part of the Alpha Ridge, a gravity corer equipped with a short core barrel segment of five meters was used to get pre-Quaternary sediments/basaltic basement. The recovery of these cores PS51/040-1 to PS51/045-1 range between zero and 1.7 meters (Figs. 11 and 13). At the Lomonosov Ridge four sediment cores PS51/058-3, PS51/065-1, PS51/067-1 and PS51/067-2 with lengths between 1 and 6 meters were recovered (Figs. 11 and 13). The lithostratigraphy described below is mainly based on the lithological core description (see Appendix) and smear slide estimates as well as MSCL data.

#### Alpha Ridge

The predominant lithology of the Alpha Ridge sediment cores is silty clay of brown, light to dark yellowish brown, and light olive brown colours. In the upper about 0.5 to 1.4 m of the cores, more sandy intervals and mud clasts occur. The most prominent features of all cores are colour cycles of light olive brown and brownish

yellow/yellowish brown sediments occurring down to the bottom of the cores. These distinct colour cycles seem not to be related neither to changes of grain-size or composition. Most of the sediments are slightly to moderately bioturbated. The main sedimentary components are quartz, feldspar and mica. In few layers detrital carbonates are enriched. Biogenic components are always rare contributing less than 1 % to the components. Near-surface sediments which usually are dark brown silty clays contain slightly higher amounts of microfossils including planktic and benthic foraminifera, fragments of radiolarian and diatoms. Rare sponge spicules were observed.

For the cores PS51/034-4 and PS51/038-4 (including GKG PS51/038-3) a more detailed study of the composition of the sediments were performed, using smear-slide analysis (Figs. 18 to 20; Table 13 to 15) and IRD counts (Fig. 21). Based on smear-slide estimates, terrigenous (mineral) particles are predominant, with the only exception of two samples from Core PS51/038-4 where very high amounts of biogenic carbonate occur at 79 and 248 cmbsf (Fig. 20 a; Table 15). In general, the sediments consist of 30 to 60 % quartz as the most dominant compound. Feldspars and mica, reaching up to 25 % each, are the next important compounds. Occasionally, terrigenous carbonate (i. e., calcite and dolomite) may reach values of 10 - 20 %. Heavy minerals occur in very variable amounts (1 - 30 %; Tables 13. - 15). In the heavy mineral fraction, amphiboles and pyroxenes are the dominant components (Figs. 18 b - 20 b; Tables 13 - 15) as already described by other authors for sediments cores from the Alpha Ridge (Darby et al., 1989 and further references therein). Both amphiboles and pyroxenes display high-amplitude variations between about 10 - 80 % and 10 - 60 %, respectively, and are generally anticorrelated (Figs. 18 b and 20 b). At Core PS51/034-4, maximum amounts of amphiboles were counted in the intervals between 5 and 50 cmbsf and below 340 cmbsf (Fig. 18 b). At Core PS51/038-4, the amphibole maxima occur between about 20 and 90 cmbsf, 160 and 200 cmbsf and below 550 cmbsf (Fig. 20 b). This suggests changes in terrigenous sediment supply from different source areas. Fe-Mn nodules occur in significant amounts in the sediments from Core PS51/038-4 at depth intervals of about 100 - 150 cmbsf, 250 cmbsf, and 530 - 630 cmbsf (Fig. 20 b).

According to the counts of IRD in X-radiographs, distinct variations in the supply of coarse-grained material by icebergs is suggested. There is a general trend towards higher IRD values in the upper part of the sedimentary sequences of cores PS51/030-1, PS51/034-4, and PS51/038-4 (Fig. 21). Based on a first rough stratigraphic framework (see below), increases in IRD input probably occur at about 1.6 Ma and 1.2 Ma.



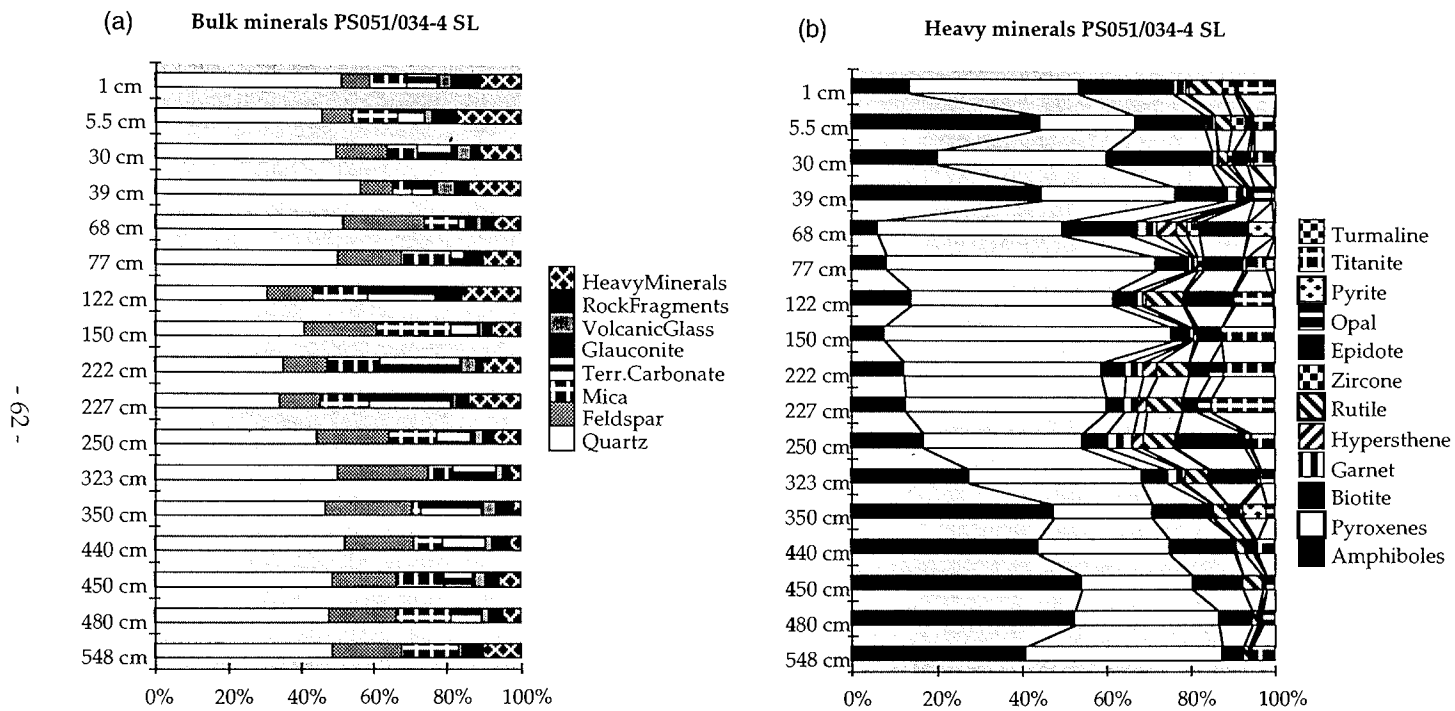


Fig. 18: Bulk (a) and heavy (b) mineralogy of sediments from gravity core (GKG) PS51/034-4, based on smear-slide counts.

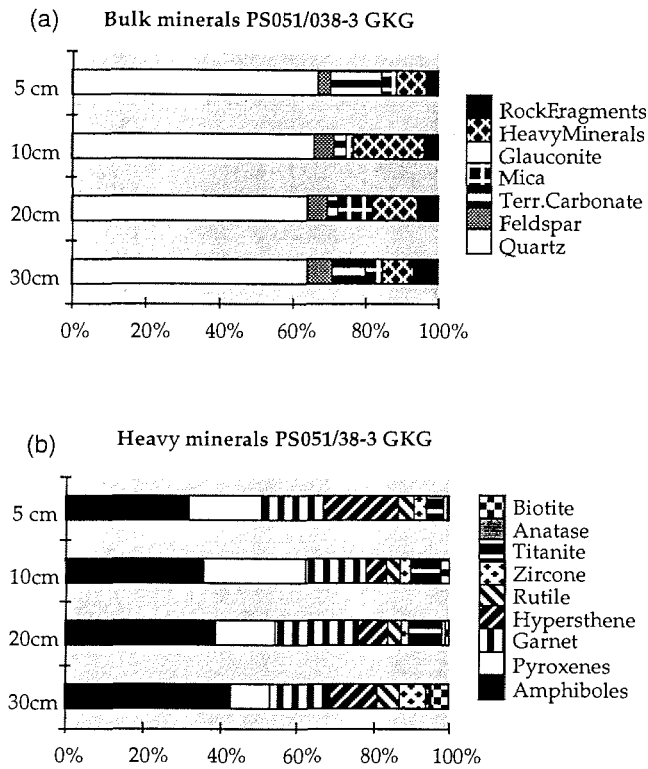


Fig. 19: Bulk (a) and heavy (b) mineralogy of sediments from giant box core (GKG) PS51/038-3, based on smear-slide counts.

In order to discuss the new records obtained during the Cruise ARK-XIV/1a in context with other sedimentary records already available from the Alpha Ridge area and to get a rough stratigraphic framework, the lithology of cores PS51/034-4, PS51/030-1 and PS51/038-4 are related to the "Standard Arctic Lithological Units" and the paleomagnetostratigraphy published by Clark et al. (1980), Jackson et al. (1985), Mudie and Blasco (1985), Jones (1987), and Darby et al. (1989) (Fig. 22). Based on this correlation, the upper standard units F to M can be identified in the sedimentary sequences of the three cores. At Core PS51/034-4, the Brunhes/Matuyama boundary and the base of the Jaramillo Event are probably at about 0.75 and 1 mbsf, respectively. The resulting sedimentation rates are about 1.2 mm/ky in the upper part (i. e., units H to M) and about 2 mm/ky in the underlying interval (units G and F). This agrees well with similar estimates of sedimentation rates by Darby et al. (1989) from this area. Using the sedimentation rate of 2 mm/ky, the extrapolated age of the base of Core PS51/034-4 is about 3.5 Ma. At cores PS51/030-1 and PS51/038-4, the sedimentation rates appears to be higher by a factor of 2 - 3 in comparison to Core PS51/034-4 (Fig. 22).

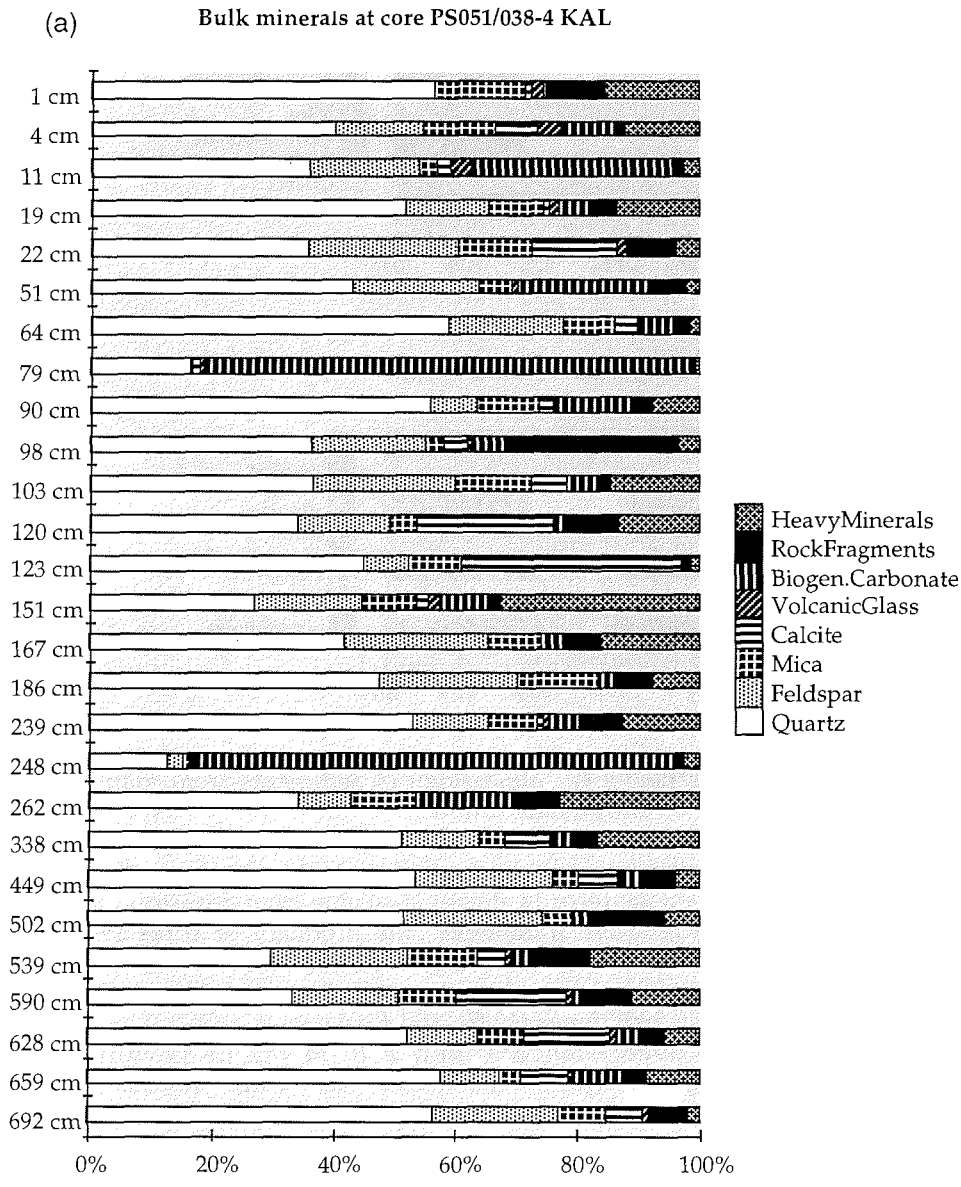


Fig. 20 a: Bulk (a) and heavy (b) mineralogy of sediments from kastenlot core PS51/038-4, based on smear-slide counts.

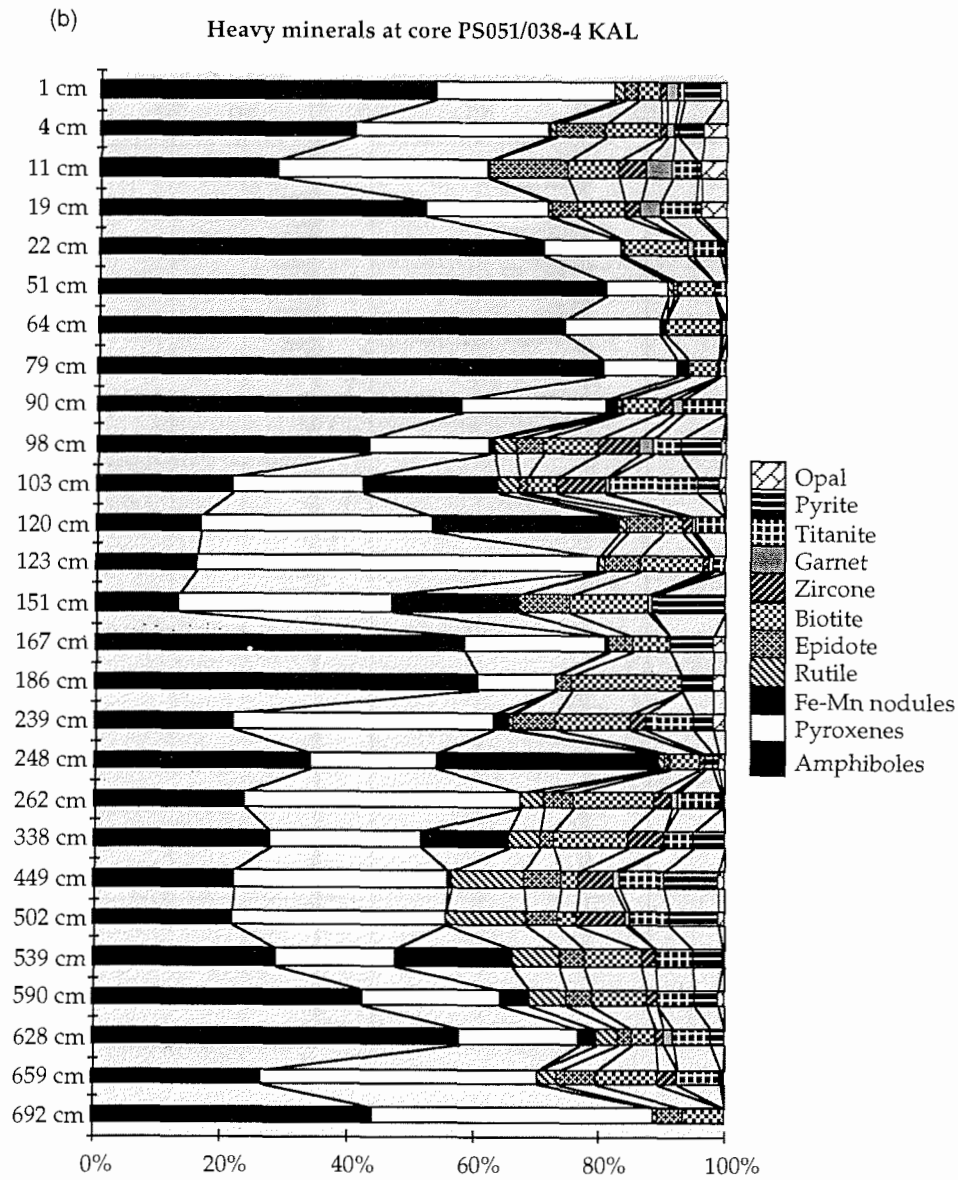


Fig. 20 b: Bulk (a) and heavy (b) mineralogy of sediments from kastenlot core PS51/038-4, based on smear-slide counts.

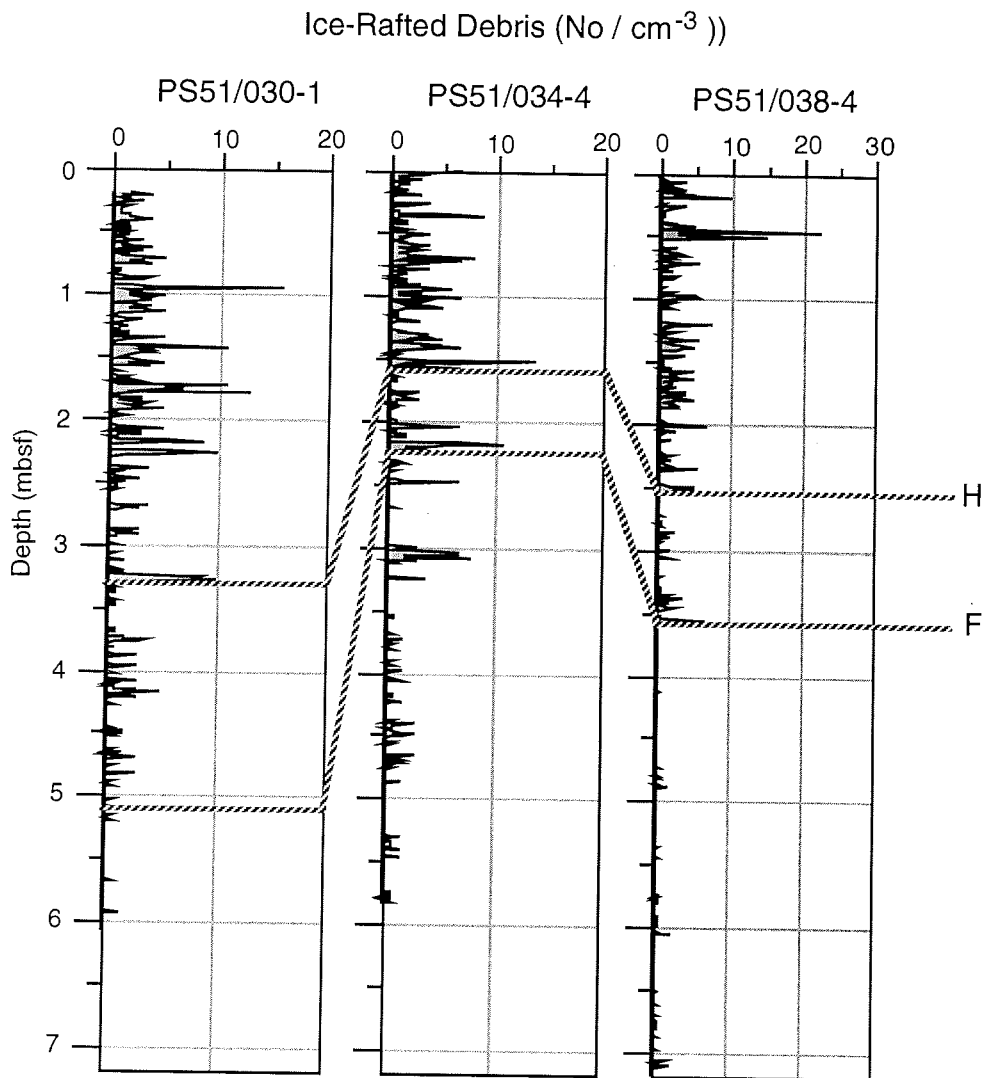


Fig. 21: Content of ice-rafted debris > 2 mm, counted in X-radiographs and expressed as numbers per 10 cm<sup>-3</sup>. Correlation lines are based on magnetic susceptibility and lithology records and indicate the basis of Standard Arctic Lithological Units H and F with an estimated age of 1.25 Ma and 1.6 Ma, respectively (cf. Fig. 22)

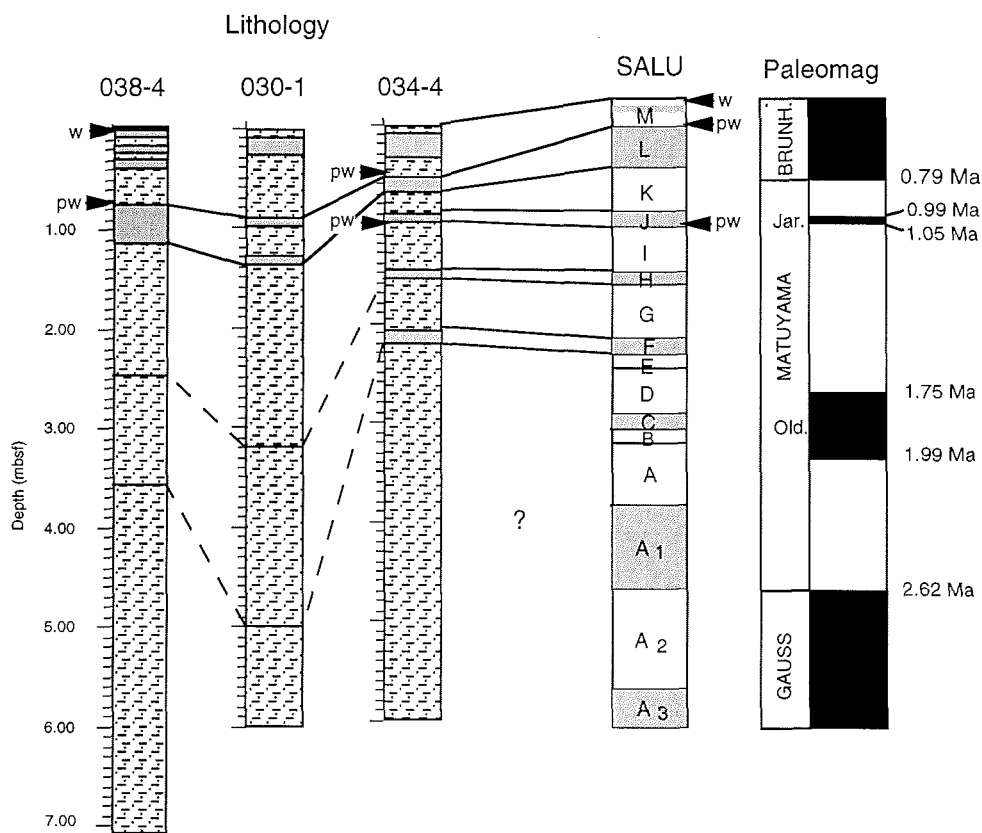


Fig. 22: Lithostratigraphy of cores PS51/030-1, PS51/034-4 and PS51/038-4, based on the lithological core description. Gray intervals in the lithology column indicate more sandy and mud clast intervals. The lithology columns are correlated with the Standard Arctic Lithological Units (SALU) and the paleomagnetostratigraphy (Clark et al., 1980; Mudie and Blasco, 1985; Jones, 1987; Darby et al., 1989); paleomagnetic time scale according to Cande and Kent (1992). Units A3, A2, C, F, H, J, L, and parts of M are more sandy intervals. "w" and "pw" indicate white and pink-white layers which can be used for core correlation. The stippled correlation lines are based on the magnetic susceptibility records.

Tab. 13: Bulk (a) and heavy (b) mineralogy of sediments from Core PS51/034-4, based on smear-slide estimates.

(a)

PS051/034-4 SL	548 cm	480 cm	450 cm	440 cm	350 cm	323 cm	250 cm	227 cm	222 cm	150 cm	122 cm	77 cm	68 cm	39 cm	30 cm	5.5 cm	1 cm
Quartz	48.9	47.9	48.6	52.1	46.8	50.4	44.6	34.2	35.2	41.1	30.6	50.1	51.6	56.3	49.8	45.8	51
Feldspar	18.8	18.5	17.9	18.9	23.8	24.8	19.8	11.2	12.2	19.8	12.6	17.6	22.3	8.9	13.8	8.3	7.9
Mica	15.5	14.9	12.8	7.8	2.4	6.8	12.8	13.4	14.6	20.3	15.2	13.8	9.4	5.3	8.6	12.5	10.3
Glauconite	0	0	0.2	0.1	0.1	0.3	0.6	0.4	0.2	0.5	3.7	2.1	2.8	0.8	1.5	0	0.3
Volcanic Glass	1.2	1.8	2.9	1.8	3.7	1.8	2.7	1.2	4.3	0.9	0.3	0.9	1.8	5.2	3.8	1.7	3.4
Terr. Carbon.	7.6	8.5	7.9	11.7	16.8	11.3	9.6	22.5	21.8	7.3	18.6	3.3	1.9	5.9	9.3	7.5	8.4
Rock Fragm.	5.8	3.7	4.3	4.8	4.5	1.9	2.6	3.4	1.7	2.4	3.4	2.1	2.9	3.9	2.3	6.9	7.8
Heavy Minerals	9.8	4.7	5.4	2.8	1.9	2.7	7.3	13.7	10	7.7	15.6	10.1	7.3	13.7	10.9	17.3	10.9

(b)

PS051/034-4 SL	548 cm	480 cm	450 cm	440 cm	350 cm	323 cm	250 cm	227 cm	222 cm	150 cm	122 cm	77 cm	68 cm	39 cm	30 cm	5.5 cm	1 cm
Amphiboles	41	52.8	54.4	43.7	47.6	27.8	16.7	12.7	12.4	7.6	14.1	8.2	5.9	44.9	20.1	44.4	13.5
Garnet	0	0	0	0.4	1.2	3.2	6.4	3.3	4.2	0.3	2.7	0.9	6.1	4.7	1.4	2.4	2.9
Hypersthene	0	0	0	0.2	0	0.9	2.5	2.1	3.1	0.4	0.9	0.2	4.6	0.2	0.2	0.2	0.9
Rutile	1.3	1.3	4.2	2.2	3.3	5.4	7.4	8.2	7.8	0.9	8.8	0.9	2.3	0.7	2.1	3.8	7.8
Zircon	0	0.2	0	0.1	0	0.5	0.3	0	0	0.8	0.3	1.3	3.1	0.4	1.3	3.2	2.8
Titanite	5.3	3.1	2.1	4.1	2.1	3.2	5.4	15.2	12.1	12.7	9.2	4.3	0.4	0.6	4.2	4.5	8.9
Pyroxenes	46.6	33.7	26.2	31.2	23.4	40.7	37.5	47.5	46.6	67.8	47.7	63.3	44	31.5	40.2	22.3	39.8
Biotite	4.8	8.1	12.1	15.3	13.2	6.1	5.8	4.2	5.7	3.9	4.1	8.3	16.2	11.4	24.7	16.6	22.6
Epidote	0.8	0.7	0.9	2.1	3.1	11.2	16.5	3.5	4.8	5.6	11.5	9.6	11.3	1.2	3.3	1.1	0.8
Turmaline	0	0	0	0	0	0.1	0.2	0	0	0	0.3	2.2	0	0.1	0.6	0.6	0
Opaque	0.2	0.1	0.1	0.1	0.9	0.9	1.1	3.3	3.3	0	0.1	0	0.2	4.1	0.7	0.4	0
Pyrite	0	0	0	0.6	5.2	0	0.2	0	0	0	0.3	0.8	5.9	0.2	1.2	0.5	0

Tab. 14: Bulk (a) and heavy (b) mineralogy of sediments from Core PS51/038-3, based on smear-slide estimates.

(a)

PS051/38-3 GKG	30 cm	20 cm	10 cm	5 cm
Quartz	64.1	64.2	65.8	67.1
Feldspar	6.8	5.3	5.4	3.1
Mica	4.6	9.7	1.8	4
Glauconite	0	0.1	0.1	0.2
Ferr. Carbonate	9.2	2.7	3.6	14.3
Rock Fragments	6.7	5.7	3.8	3.2
Heavy Minerals	8.6	12.3	19.5	8.1

(b)

PS051/38-3 GKG	30 cm	20 cm	10 cm	5 cm
Amphiboles	42.8	38.8	35.4	31.6
Garnet	15.9	21.7	15.6	16.2
Hypersthene	12.4	7.4	5.4	19.6
Rutile	5.7	3.7	3.6	3.9
Zircone	7.2	2.2	2.8	3.2
Titanite	0.8	8.6	7.7	4.7
Anatase	0.2	0.8	1.1	1.2
Pyroxenes	10	15.6	26.8	19.1
Biotite	5	1.2	2.7	0.5



Tab. 15 a: Bulk (a) and heavy (b) mineralogy of sediments from Core PS51/038-4, based on smear-slide estimates.

(a)

PS051/038-4 KAL	692 cm	659 cm	628 cm	590 cm	539 cm	502 cm	449 cm	338 cm	262 cm	248 cm	239 cm	186 cm	167 cm	151 cm
Quartz	56.7	57.8	52.2	33.1	29.5	51.8	53.4	51.2	34.1	12.6	52.9	47.5	41.6	26.9
Feldspar	20.3	9.4	11.7	17.6	22.8	22.8	22.6	12.9	8.9	2.5	12.7	22.8	23.8	17.6
Mica	7.8	3.8	7.9	9.8	11.7	4.7	4.6	4.1	10.6	0.9	7.8	13.3	8.7	8.8
Calcite	5.9	7.8	13.9	17.9	4.6	5.3	6.2	7.6	0	0.3	0.9	0	0	2.2
Volcanic Glass	0.9	0.8	0.6	0.8	0.8	0.4	0.2	0.3	0.1	0.6	1.3	0.3	0	1.9
Biogen Carbonate	0.6	7.9	4.5	1.9	2.9	2.5	3.3	3.8	16.7	79.8	4.8	2.9	3.9	8.8
Rock Fragments	5.9	3.9	3.3	7.9	9.8	11.9	5.9	3.6	6.9	0.7	6.9	5.3	5.9	1.2
Heavy Minerals	1.9	8.6	5.9	11	17.9	5.9	3.8	16.5	22.7	2.6	12.7	7.9	16.1	32.6

- 70 -

123 cm	120 cm	103 cm	98 cm	90 cm	79 cm	64 cm	51 cm	22 cm	19 cm	11 cm	4 cm	1 cm
44.9	33.9	36.6	36.1	55.8	16.2	58.9	42.9	35.5	51.7	35.9	39.9	56.7
7.4	15.2	23.3	18.8	7.5	0.3	19	21.1	25.1	13.8	17.9	14.7	17.7
8.6	4.6	12.6	3.1	10.6	0.2	8.2	5.4	11.8	9	3.1	11.9	14.8
36.1	22.5	5.7	3.9	2.2	0.9	3.7	0.1	13.9	0.9	2.1	6.9	1.1
0	0	0.2	0.9	0	0.7	0	0.8	1.7	1.7	3.5	3.9	2.1
0.9	1.8	4.9	5.7	12.9	80.1	6.8	21.7	0.2	5.3	33.1	9.7	0.7
0.9	8.9	2.2	27.9	3.3	0.8	1.6	5.9	7.9	3.9	1.8	0.9	8.9
1.2	13.1	14.5	3.6	7.7	0.8	1.8	2.1	3.9	13.7	2.6	12.1	15.7

Tab. 15 b: Bulk (a) and heavy (b) mineralogy of sediments from Core PS51/038-4, based on smear-slide estimates.

(b)

PS051/038-4 KAL	692 cm	659 cm	628 cm	590 cm	539 cm	502 cm	449 cm	338 cm	262 cm	248 cm	239 cm	186 cm	167 cm	151 cm
Amphiboles	43.9	26.4	57.9	42.5	28.7	21.7	22.2	27.8	23.7	33.9	21.8	60.6	58.3	13
Garnet	0	0.1	1.8	0	0	0.4	0.8	0	0.9	0	0.1	0	0	0.3
Fe-Mn nodules	0	0	3.2	4.8	18.9	0.1	0.3	13.9	0	35.6	2.5	0.1	0.3	20
Rutile	0.8	3.1	3.3	5.8	7.3	12.8	11.8	4.9	3.7	0.9	0.7	0	0	0.4
Zircon	0	2.9	1	1.8	2.1	8	5.7	5.8	2.9	0.9	2.4	0	0	0.1
Titanite	0	6.9	5.8	5.7	6	6.5	6.8	4.6	6.9	0.9	7.7	0	0	0
Pyroxenes	44.7	43.8	18.7	21.9	18.7	33.8	33.8	23.9	43.8	20	41.3	12.5	22.7	33.9
Biotite	6.7	9.7	3.8	8.8	9.1	3.1	2.8	11.9	12.8	4.8	11.8	17.8	5.9	12.5
Epidote	3.9	6.5	2.1	3.9	4.1	4.9	5.9	2.2	4.7	0.8	6.7	2.2	3.8	7.9
Opaque	0	0.4	0.3	1	0.5	0.9	1.1	0.1	0.4	1	2.1	2	2.1	0
Pyrite	0	0.2	2.1	3.8	4.6	7.8	8.8	4.9	0.2	1.2	2.9	4.8	6.9	11.9

- 71 -

123 cm	120 cm	103 cm	98 cm	90 cm	79 cm	64 cm	51 cm	22 cm	19 cm	11 cm	4 cm	1 cm
15.7	16.5	21.5	43.2	57.9	80.6	74.3	80.8	71.1	51.8	28.5	40.6	53.3
0.9	0.7	0.8	1.7	1.6	0.6	0.7	0	0.9	2.9	4.1	1.1	1.9
0.3	29.9	21.7	1.2	1.9	2.2	0.9	0	0	0	0.2	0.1	0
0.9	1.3	3.5	3.1	0.9	0	0	0.9	0	0.7	0.1	1.2	1.7
0.9	1.4	7.8	6.9	2.1	0	0.4	0	0	2.5	4.2	0.9	0.9
1.7	4.7	13.9	4.5	6.9	0.9	0	2.2	4.3	5.9	4.2	0.9	0.7
64	36.6	20.5	18.9	22.9	11.3	14.8	9.8	11.9	19.6	33.3	30.9	28.7
9.9	3.3	4.6	8.8	5.7	4.4	8.9	5.6	9.9	7.5	8.3	8.9	3.7
5.6	5.6	1.3	4.3	0.1	0	0	0.7	0.7	4.1	12.5	7.7	2.1
0	0	1.1	0.6	0	0	0	0	0.5	4.1	4.1	3.8	1.2
0.1	0	3.3	6.8	0	0	0	0	0.7	0.9	0.5	3.9	5.8

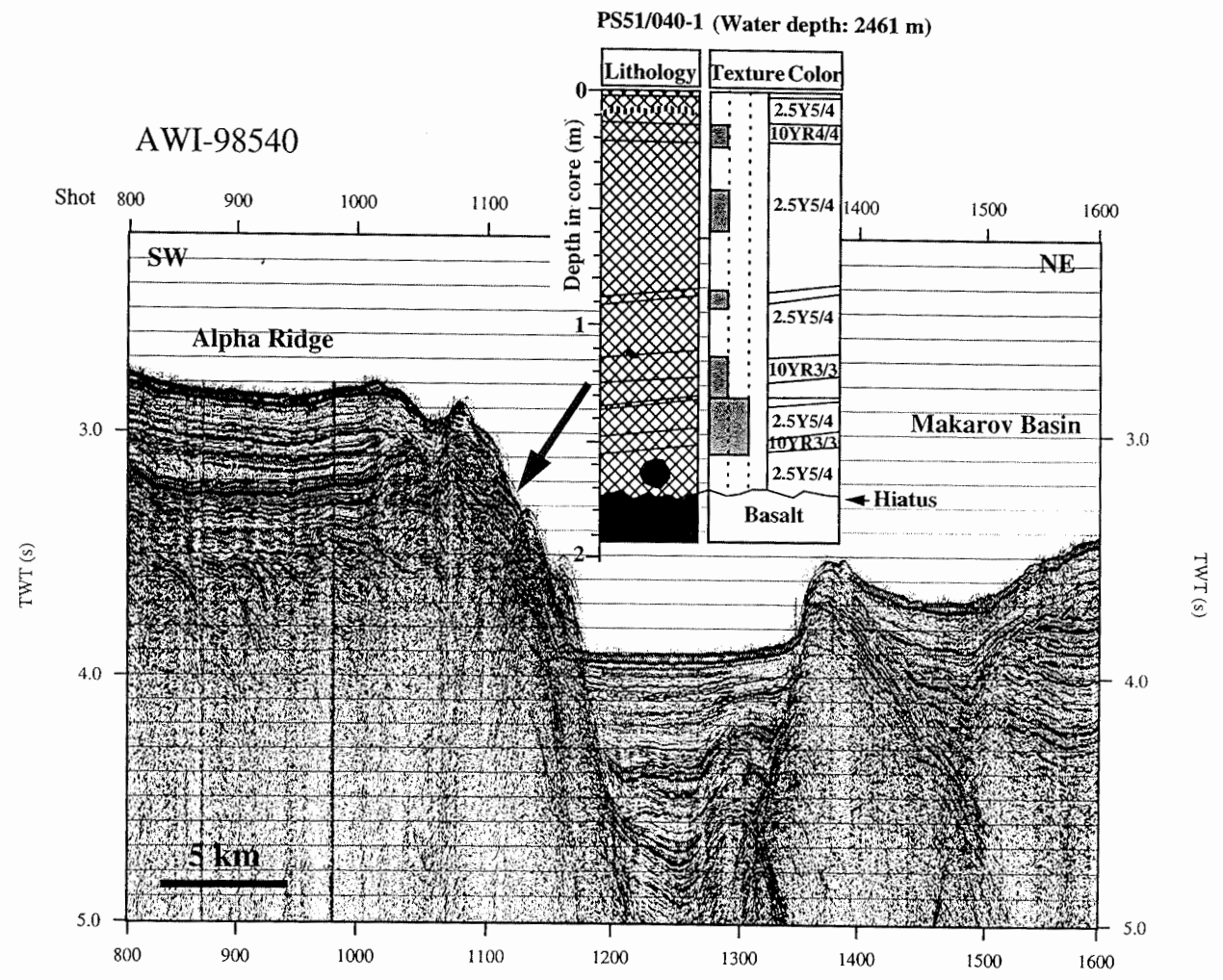
#### Graben in the westernmost part of the Alpha Ridge

At the steep slope of a graben-like structure in the westernmost part of the Alpha Ridge the Seismic Profile 98540 suggests that older sediment strata and/or basaltic basement are cropping out (Fig. 23). Thus, a coring program was carried out to try getting pre-Quaternary sediments/basaltic basement. In four of the cores (PS51/040-1, PS041-1, PS51/042-1 and PS51/043-1; cf., Fig. 11), pieces of basalts were recovered. From these cores, only Core PS51/040-1 was opened and described yet. In this core, a large piece of basalt (7 cm in diameter) was found at 160 - 166 cmbsf; the core catcher contains further pieces of basalt. The overlying sediments are dark brown, light olive brown to yellowish brown silty clays with some amounts of sand and mud clasts in the uppermost part (Fig. 23), i. e., very similar to those recovered in cores PS51/30-1 to PS51/038-4 (see above). Thus, the age of the sediments is probably Quaternary and a major hiatus should occur between basalts and overlying sediments. Further more detailed investigations of the basalts as well as the sediments of the up to now unopened sediment cores will hopefully allow to date the basalts and to study the Quaternary (/pre-Quaternary?) paleoenvironmental history of the Alpha-Ridge area.

#### Lomonosov Ridge

During the cruise track along the Lomonosov Ridge RV POLARSTERN crossed a steep, north-south striking slope at about 81° 50'N, 140° 30'E where older sediments may crop out. From this slope, gravity cores PS51/067-1 and PS51/67-2 (Fig. 11) with a length of 1 and 3.7 m, respectively, were obtained. The sedimentary sequence of the long Core PS51/067-2 can be divided into three lithological units (Fig. 24). Unit III (332 cmbsf to bottom of core) consists of dark gray, firm sandy silty clay. Unit II (209 - 332 cmbsf) is an olive to light olive brown (sandy) silty clay. The upper part of this unit is slightly bioturbated. Unit I (0 to 209 cmbsf) consists of dark brown, yellowish brown and light olive brown, partly bioturbated silty clay. A pink layer occurs at 60 cmbsf. These lithological units are similar to those of sediment cores recovered from the Lomonosov Ridge during POLARSTERN Cruise ARK-XI/1 (Stein et al., 1997). The boundary between lithological units II and I coincides with a distinct jump in the porosity and wet bulk density suggesting a hiatus at that depth (Fig. 24). The lowermost Unit III may be of Oxygen Isotope Stage 6 age, based on the correlation with the ARK-XI/1 cores (Stein et al., 1997). Whether this age correlation is correct or whether the sedimentary sequence even represents older time intervals has to be verified by further more detailed investigations.

Fig. 23: Seismic profile 98540 and location and lithology of Core PS51/040-1. At 1.73 mbsf, the gravity corer stucked in the basalt.



PS5/067-2

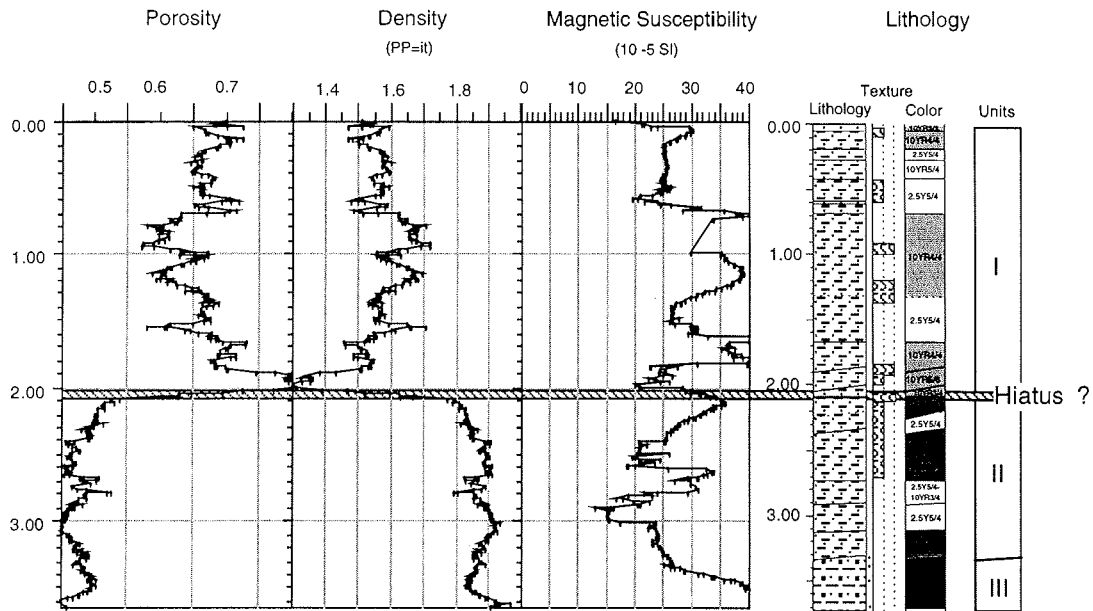


Fig. 24: Lithology and porosity, wet bulk density, and magnetic susceptibility records from Lomonosov Ridge Core PS51/067-2. Roman numerals indicate lithological units.

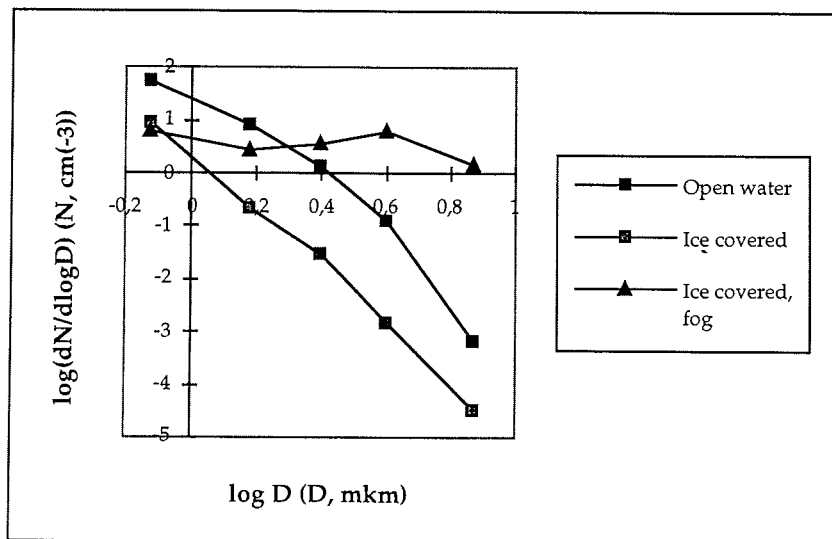


Fig. 25: Typical aerosol particle size distribution in the study area. Series: 1 - over the open water; 2 - over the ice covered sea; 3 - over the ice covered sea during fog condition.

### 3.6 Aerosols (V. Shevchenko)

Numerous studies have shown that aerosols in the Arctic are of importance for atmospheric chemistry and climate (Barrie, 1986). But up to now aerosols in the marine boundary layer in the high Arctic have been studied little. Here, preliminary results of the studies of aerosol size distribution over the NW Barents Sea and the Central Arctic are presented. During the ARK-XIV-1a Expedition 183 measurements of aerosol size spectra at 61 sites and 14 measurements by DAES-3 were carried out (Tables 7 and 8). In general, there is a much greater number of small particles (with sizes from 0.5  $\mu\text{m}$  to 2  $\mu\text{m}$ ) in comparison to large particles, as it is described elsewhere (O'Dowd et al., 1997). The observed particle size spectra are on whole conservative to changes of temperature, relative humidity, wind velocity and direction. In ice-covered areas we find much lower concentrations of particles from all size classes (Fig. 25). This could testify the input of sea salt particles from the sea surface microlayer by wind and the importance of these particles for the chemical composition of marine aerosols, as it has been shown in other regions (O'Dowd et al., 1997). We shall see the input of wind blown sea salt after the elemental analysis of aerosol samples in home laboratory. During a fog formation concentration of large particles (from 3 to 5  $\mu\text{m}$ ) sharply increased as it has been found in the Laptev Sea (Smirnov et al., 1997). A more detailed study of the parameters of aerosol size distribution and controlling factors will be carried out later in comparison with other areas.